THE DEVELOPMENT OF POROUS POLYMERIC SURFACES FOR SCREENING ACYLCARNITINES BY LASER DESORPTION IONIZATION MASS SPECTROMETRY

By

MICHAEL WILLIAM BELFORD

A DISSERTATION PRESENTED TO THE GRADUATE SCHOOL
OF THE UNIVERSITY OF FLORIDA IN PARTIAL FULFILLMENT
OF THE REQUIREMENTS FOR THE DEGREE OF
DOCTOR OF PHILOSOPHY

UNIVERSITY OF FLORIDA

2003

For William

ACKNOWLEDGEMENTS

I would like to begin by extending my sincerest thanks to Dr. Richard A. Yost for his guidance and support throughout my career at the University of Florida. Not only did he offer insight to the work described in this dissertation he allowed me to discover what I want to do when I grow up. For that, I am eternally grateful. My committee members, Dr. James Winefordner, Dr. David Powell, Dr. John Eyler and Dr. Bruce Goldberger, were also of great assistance to me throughout my time at the university and I am very appreciative. I owe a debt of gratitude to Dr. George Stafford at Thermo Finnigan for helping fund my work during my graduate career and providing me with hands-on experience in industry, not to mention my first trip to California.

The Yost group members, both present and past, will always hold a special place in my heart. It was a joy to work with Alisha, Tim, Bill, Samaret, Chris, Hong and Hidee. I look forward to seeing each of them for years to come at conferences and group dinners. A special thank you goes to Dr. James Murphy, Todd Hunt, Leonard Rorrer and honorary group member, TJ Baniauskas. It was worth the trip to Gainesville just to get to know them.

My parents, Hal and Emelia Belford, deserve so much of the credit for my success. Their constant encouragement has always given me the desire to push on, even when things got tough.

Finally I can trace all good things in my life back to the day I met my best friend Shana Without her and William none of this would have had any value I will always consider convincing her to spend her life with me as my grandest achievement

TABLE OF CONTENTS

LIST OF FIGURES

Abstract of Dissertation Presented to the Graduate School
of the University of Florida in Partial Fulfillment of the
Requirements for the Degree of Doctor of Philosophy

THE DEVELOPMENT OF POROUS POLYMERIC SURFACES FOR SCREENING ACYLCARNITINES BY LASER DESORPTION IONIZATION MASS SPECTROMETRY

By

Michael William Belford

May 2003

Chairman: Richard A. Yost
Major Department: Chemistry

Laser desorption ionization techniques such as matrix-assisted laser desorption/ionization mass spectrometry (MALDI-MS) have traditionally employed an organic matrix to enhance ionization efficiency of a sample. The matrix plays a major role in the ionization process by spatially separating the analyte molecules, absorbing laser energy, and donating protons to the analyte in the ion plume. However, a major drawback to MALDI-MS is the intense low mass-to-charge ion background that arises from the organic matrix. Matrix-free laser desorption techniques have been recently introduced in which the sample surface plays the role of the organic matrix without producing the high chemical background. With desorption/ionization on porous silicon (DIOS), the analyte is

spotted on electrochemically etched porous silicon and no additional organic matrix is added. The resulting mass spectra are similar to MALDI spectra but without the organic matrix background. However, the production of porous silicon is not entirely reproducible, which can lead to inconsistent MS data. The development of a new matrix-free laser desorption technique, called aerogel MALDI, is first reported here.

Aerogels are highly porous polymeric solids produced by cross-linking a colloidal dispersion of dissolved monomeric precursors. The resulting rigid gel is supercritically dried to avoid densification of the pore system; the resultant aerogel is highly porous and easily reproduced. The composition of the aerogel can be precisely controlled, and custom surfaces can be produced by selecting specific monomers or by modification of the surface after polymerization. Here, resorcinol-formaldehyde (RF) aerogels are characterized as organic-matrix free substrates for laser desorption on a quadrupole ion trap mass spectrometer.

To test the quantitative ability of the aerogel MALDI technique in the analysis of small biomolecules, the biomarkers attributed to the metabolic disorder medium-chain acyl-CoA dehydrogenase deficiency (MCADD), l-carnitine and octanoylcarnitine, were analyzed. In order to screen for MCADD, the relative concentration of the biomarkers must be determined from whole blood samples. For this, calibration curves were generated using an internal standard, for each compound and compared to curves produced by MALDI-MS analysis.

CHAPTER 1
INTRODUCTION

Biomarker Screening

The term "screening" refers to the application of a medical procedure or test to patients who have no symptoms of a particular disease in order to determine their potential of having the disease. The screening procedure itself does not diagnose the illness: those who have a positive result from the screening test will need further evaluation with subsequent diagnostic tests. The goal of the screening procedure is therefore to reduce morbidity or mortality from the disease by detecting diseases as early as possible so that subsequent treatments have a chance of success.

Sensitivity and specificity are the major measures of a test's ability to correctly classify a person as having a disease or not having a disease. Sensitivity refers to the test's ability to designate whether an individual with disease will give a positive result. A highly sensitive test is important so that there are no false negative results. This is critical because individuals with negative results to the test should be confident that they do not have the disease and therefore do not require further treatment. The test's specificity has to do with its ability to verify that an individual does not have the disease. A highly specific test is important so that there are few false positive results. It is not feasible for a test with low specificity to be used for screening, since individuals without the disease

could inaccurately screen positive leading to further unnecessary diagnostic procedures

Metabolic Disorders

Approximately one out of every 1 500 babies born in the United States each year has a detectable metabolic disorder (Elliman *et al* 2002) These disorders can cause mental retardation, physical impairment and/or death However, in most cases these complications can be prevented or significantly reduced in severity with early diagnosis and treatment

Medium-chain acyl-CoA dehydrogenase deficiency (MCADD) is an inherited metabolic disorder occurring in one in every 10 000 live births The disorder is characterized by an increase in the acylcarnitine octanoylcarnitine in blood and urine (Wang *et al*., 1999) Due to a deficiency of MCAD activity, patients cannot metabolize their stored fat and are therefore at risk while fasting or when suffering from infection Approximately 25% of patients affected by MCADD die during the first instance of symptoms which include low blood sugar, seizures and cardiac arrest. Although there is presently no cure for MCADD, the disorder can be easily controlled after diagnosis through diet and carnitine supplementation

At present, tests for MCADD and a number of other metabolic disorders are not routinely given to newborns in the nation In order to test for MCADD, the ratio of octanoylcarnitine to l-carnitine must be determined In patients with normal metabolic function, the concentration in blood of l-carnitine ranges from twenty to eighty micromolar The concentration of octanoylcarnitine in blood is

typically four times lower than the concentration of l-carnitine ranging from five to twenty micromolar in individuals with normal metabolic function Although there is a broad range of concentrations for these biomarkers it is the ratio of acylcarnitine to free carnitine that is important to the screening process A molar ratio of octanoylcarnitine to free carnitine of less than 0.25 in blood is characteristic of individuals with normal metabolic function In cases of metabolic disorder this ratio is elevated as high as 1 00 due to an increase in the concentration of octanoylcarnitine (Chen & Millington 2000)

L-Carnitine

L-carnitine (3-hydroxy-4-*N*-trimethylaminobutyrate) facilitates the metabolism of long-chain fatty acids in the human body by transporting fatty acid acyl- groups across mitochondrial membranes as acylcarnitine esters (Borum 1998) Without l-carnitine fatty acids could not cross the membrane and energy would not be produced for the body through fatty acid oxidation L-carnitine also assists with the removal of short- and medium-chain fatty acids out of the mitochondria These fatty acids are products of β-oxidation of long-chain fatty acids and are toxic if not removed Once these toxic fatty acids have been removed from the mitochondria the l-carnitine level outside the membrane is restored and the process can be repeated

L-carnitine is synthesized from the amino acids lysine and methionine in a series of reactions shown in Figure 1-1 (Rebouche & Broquist 1976) Synthesis begins with lysine undergoing three consecutive methylation reactions with S-adenosylmethionine (SAM) acting as the methyl donor The resulting

trimethyllysine is reacted with α ketoglutarate and ascorbic acid in the presence of oxygen and iron to form hydroxy-trimethyllysine

Trimethylaminobutyraldehyde is then formed from the reaction of hydroxy-trimethyllysine with pyridoxal 5 -phosphate (vitamin B6) Trimethylaminobutyrate is then formed by way of a reaction requiring NADH Finally the trimethylaminobutyrate is hydroxylated into carnitine with α-ketoglutarate and ascorbic acid in the presence of oxygen and iron (Rebouche & Broquist 1976)

Figure 1 2 shows the process of transferring fatty acids across the mitochondrial membrane Fatty acids are present outside the mitochondria as esters of coenzyme A (acyl-CoA) Acylcarnitines are formed when these fatty acid esters are trans-esterified to L-carnitine by the enzyme carnitine palmitoyltransferase I at the mitochondrial membrane (Rebouche & Broquist 1976) Acylcarnitines are then able to enter the mitochondria by way of a carnitine carrier protein Once in the matrix of the mitochondria the fatty acids are released to undergo β-oxidation This leaves the remaining carnitine free to pick up fatty acid byproducts of metabolism (short- and medium-chain fatty acids) inside the matrix and exit the mitochondria by the process mentioned above

Testing

In the state of Florida there are approximately 195,000 births every year. For each of these births blood is collected from a small needle prick on the heel of the newborn within the first two days after birth The blood is collected directly on a filter paper card in a series of five spots and is allowed to dry for use in future analysis From these samples the state of Florida requires screening for

congenital adrenal hyperplasia (CAH), galactosemia, hypothyroidism and phenylketonuria (PKU). For infants of African-American descent, a test for sickle cell disease (SCD) is also required (Chace *et al.* 2002.) Figure 1-3 is a map showing which states offer supplemental screening for other disorders by tandem mass spectrometry methods.

Although testing for MCADD and most other metabolic disorders is not yet required by many states, including the state of Florida, a handful of research groups are studying these diseases in hopes of finding an efficient methods for screening. Procedures being implemented include radiometric methods (Engel *et al.* 1981), separation techniques, such as high performance liquid chromatography with ultraviolet detection (HPLC-UV) (Kagawa *et al.* 1999), and a number of separation techniques coupled to mass spectrometry (MS) such as liquid chromatography (LC-MS) (Shigematsu *et al.*, 1999), capillary electrophoresis (CE-MS) (Helnig & Henion, 1999) and gas chromatography (GC-MS) (Kuhara *et al.* 1999).

Mass spectrometry is useful in the analysis of biomarkers because it is more specific than the other methods by themselves. For example, radiometric methods are capable of determining total carnitine concentration, but cannot differentiate between free carnitine and each individual acylcarnitine present in a sample. Similarly, HPLC with UV detection can separate free carnitine and each of the acylcarnitines, but cannot correlate the resulting peaks in the chromatogram without running a series of standards first and comparing

retention times. Even then, HPLC-UV cannot differentiate between co-eluting compounds.

When coupled to mass spectrometry, these chromatographic techniques are capable of compound-specific detection. However, l-carnitine and acylcarnitines are not amenable to electron ionization (EI) or chemical ionization (CI) techniques due to both their zwitterionic character and their thermally labile functional groups. Therefore, carnitine samples must be derivatized before they can be analyzed by any of the MS methods described above (Carlson, 1996).

Adding another stage of mass spectrometry, known as tandem mass spectrometry (MS/MS), adds further selectivity to the analysis (Yost & Fetterolf, 1983). In MS/MS, an ion selected in the first stage of MS can be fragmented in order to produce a mass spectrum of its fragment ions, known as a daughter spectrum. This spectrum is composed of only fragment ions corresponding to the ion selected in the first stage of MS, and thus can give structural information as well as assure the user of the identity of the compound detected. For carnitine analysis, tandem mass spectrometry techniques include GC/MS/MS (Woffendin, 1999), LC/MS/MS (Johnson *et al.*, 1998) and electrospray ionization MS/MS (McClellan *et al.*, 1997).

Fast atom bombardment mass spectrometry (FAB-MS) became a popular technique for analyzing carnitines in the late 1980s and 1990s due to its role in identifying and characterizing acylcarnitines as biomarkers in the urine of children with propionic academia, methylmalonic acidura and Reye's Syndrome for the first time (Millington *et al.*, 1984). FAB-MS is a soft ionization technique that

works well with ionic species such as carnitines. For FAB-MS analyses, the sample is dissolved in a non-volatile liquid matrix, generally glycerol, and a neutral argon atom beam (or an argon ion or cesium ion beam) is focused onto the liquid matrix-sample solution. Ions are ejected from the surface of the liquid and into the gas phase. These gas-phase ions are then extracted from the source and into the mass analyzer (Barber *et al.*, 1982). The resulting FAB spectrum can contain extensive chemical background arising from the matrix (Ligon & Dorn, 1984). Furthermore, a number of chemical reactions can occur between the analyte and matrix while in the liquid phase, resulting in unexpected ions (Detter *et al.*, 1988). Finally, an excess of salts present in the sample can suppress the analyte ion signal (Moon & Kelley, 1988). With samples of biological origin, such as blood samples discussed here, it is therefore recommended that the sample undergo a prior cleanup step if FAB-MS is used for analysis (Li *et al.*, 1992).

Since each of the previously mentioned techniques requires extraction and derivatization of a blood spot sample from a filter paper card, plus separation time for chromatographic techniques, analysis by matrix-assisted laser desorption ionization/mass spectrometry (MALDI-MS) has also been explored (Briand *et al.*, 1995). MALDI analyses do not require significant analysis times compared to those required of chromatographic separations and also do not require derivatization of the sample. Furthermore, sample preparation time is decreased because MALDI is tolerant of salts and buffers in the analyte solution.

compared to other ionization techniques such as electrospray ionization and FAB and does not generally need a cleanup step (Beavis & Chait 1990)

However, since MALDI typically produces a large chemical background in the mass range of the biomarkers discussed here, it was advantageous to pursue organic matrix-free laser desorption techniques for these analyses Desorption ionization on porous silicon (DIOS) is such a technique and is capable of producing mass spectra similar to MALDI-MS spectra without the addition of an organic matrix to the sample (Wei *et al* 1999) Furthermore the high chemical background caused by the organic matrix is not present in DIDS-MS spectra However, the production of porous silicon is not consistant which can lead to irreproducible MS data

Overview of Dissertation

This dissertation focuses on the development of a novel porous polymeric surface known as aerogel to be used as a platform for laser desorption mass spectrometry (LD-MS) A quadrupole ion trap mass spectrometer will be used for the analyses described here Data will be shown for traditional matrix-assisted laser desorption ionization (MALDI) analyses with organic matrices as well as the matrix-free laser desorption technique desorption ionization on porous silicon (DIOS), for the analysis of small mass-to-charge biomarkers A new technique called aerogel MALDI will be introduced and emphasis will be placed on this technique for screening biomarkers of metabolic disorders

This first chapter has introduced the basic concepts of screening for biomarkers and has given an overview of metabolic disorders and current testing

methods in detection of these disorders Chapter 2 focuses on the quadrupole ion trap mass spectrometer and its function, as well as a description of the instrument used in this study An introduction to laser desorption techniques is included in this chapter as well Chapter 3 presents data acquired by MALDI-MS and DIOS-MS in the detection of biomarkers for metabolic disorders as well as establishing problems inherent to these techniques that led to the search for a novel method of detection Chapter 4 introduces aerogels focusing on their production and characteristics beneficial to LD-MS analysis In this chapter aerogels are characterized as LD MS platforms and data are shown comparing aerogel MALDI-MS with traditional MALDI-MS and DIOS-MS In Chapter 5, data are shown demonstrating the use of aerogel MALDI in the detection of the biomarkers studied in previous chapters by other techniques Comparison to these other methods is included Finally Chapter 6 summarizes the data presented in this dissertation and offers direction on future studies for aerogel MALDI analysis

Figure 1-1 Synthesis of l-carnitine from the amino acids lysine and methionine. Synthesis begins with the methylation of lysine by S-adenosylmethionine (SAM) followed by reaction with α-ketoglutarate and ascorbic acid in the presence of oxygen and iron. The product is then reacted with pyridoxal 5'-phosphate (vitamin B6) followed by a reaction requiring NADH. Finally the product is hydroxylated into carnitine with α-ketoglutarate and ascorbic acid in the presence of oxygen and iron (Rebouche & Broquist 1976)

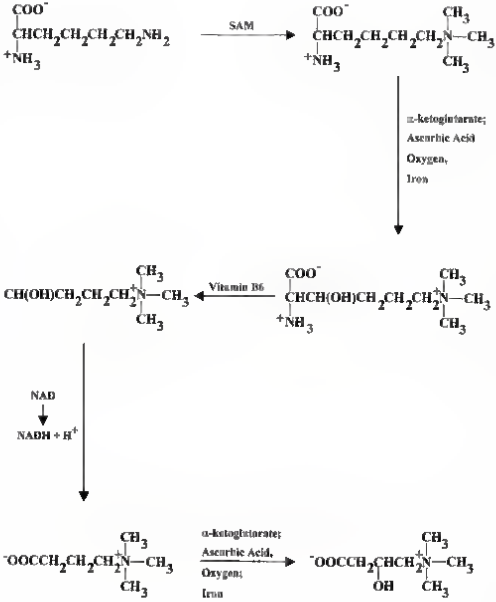
SAM
α-ketoglutarate;
Ascorbic Acid
Oxygen,
Iron
Vitamin B6
NAD
NADH + H+
α-ketoglutarate;
Ascorbic Acid,
Oxygen;
Iron

Figure 1-2 Fatty acid transfer across the mitochondrial membrane. Without l-carnitine, fatty acids could not cross the membrane and energy would not be produced for the body through fatty acid oxidation. However, when fatty acids are combined with l-carnitine to form acylcarnitines, they can pass through the membrane. L-carnitine also assists with the removal of short- and medium-chain fatty acids from the mitochondria (Rebouche & Broquist, 1976)

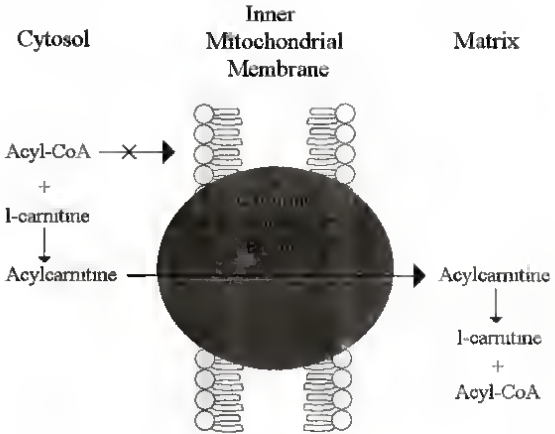
Cytosol
Inner
Mitochondrial
Membrane
Matrix
Acyl-CoA
+
l-carnitine
Acylcarnitine
Acylcarnitine
l-carnitine
+
Acyl-CoA

Figure 1-3 Metabolic disorder testing map. Testing for all metabolic disorders is not presently required by all states. However, some states do have testing programs while others offer supplemental testing through private laboratories. This map shows the availability of supplementary testing by tandem mass spectrometry in each state (Chace *et al*., 2002)

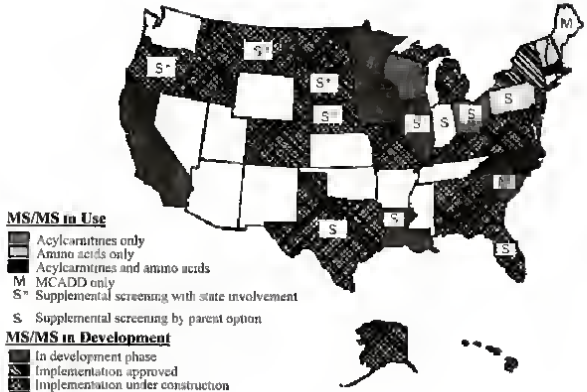
M
S*
S*
S*
S*
S
S
S
S
S
S*
S*
S
S
S
MS/MS in Use
Acylcarnitines only
Amino acids only
Acylcarnitines and amino acids
M MCADD only
S* Supplemental screening with state involvement
S Supplemental screening by parent option
MS/MS in Development
In development phase
Implementation approved
Implementation under construction
No plans

CHAPTER 2
INSTRUMENTATION

History of the Quadrupole Ion Trap

Paul and Steinwedel originally described the fundamental operation of the quadrupole ion trap (QIT) mass spectrometer as an ion storage device in 1956 (Paul & Steinwedel, 1956). This eventually led to the awarding of the Nobel Prize in Physics in 1989 to Wolfgang Paul. Over the next five decades a series of discoveries led to the ion trap becoming one of the most widely used commercial mass spectrometers in the world. Below is a brief summary of these discoveries followed in the next section by a more detailed description of ion trap fundamentals.

The first demonstration of the ion trap as a mass-selective device was by Fischer who in 1959 showed mass resolution of krypton isotopes (Fischer, 1959). In 1968 Dawson was the first to add an external detector for the detection of ions ejected through a hole in the end-cap electrode (Dawson & Whetten, 1968). In 1971, it was shown that by applying radio frequency (RF) and direct current (DC) voltages to the ring electrode, the ion trap was capable of mass-selective storage of ions (Dawson & Whetten, 1971). In 1980, resonance excitation of ions within the trap was introduced by Fulford (Fulford *et al.*, 1980). Finally, in 1985, Stafford demonstrated the ability to mass-selectively eject ions from the trap over a large mass-to-charge

(m/z) range (Stafford *et al*., 1985). This method, dubbed mass selective instability scanning, made the quadrupole ion trap a practical mass spectrometer and has led to many generations of commercial ion trap instruments.

Quadrupole Ion Trap Theory

The quadrupole ion trap, also known as the Paul trap, consists of three cylindrically symmetrical electrodes: an entrance end-cap, a ring electrode and an exit end-cap, as shown in Figure 2-1. The theoretical dimensions of the Paul trap were calculated to produce a quadrupolar field described by Equation 2-1.

$$r_o^2 = 2z_o^2 \qquad \text{EQ 2-1}$$

where r_o is the radius of the ring electrode and z_o is the distance from the center of the trap to the end-caps (March, 1995). However, for ion injection and ejection, the end-cap electrodes must have a hole in order to let ions in and out of the trap. These holes in the end-cap electrodes cause imperfections in the quadrupolar trapping field, which leads to poorly resolved mass spectra (Syka, 1995). To correct for these imperfections, the trap was stretched from the ideal geometry of $z_o = .707r_o$ to $z_o = 0.783r_o$. At this stretched geometry, the field imperfections are minimalized and resolution is improved.

For the operation of the ion trap, radio frequency (RF) and direct current (DC) voltages are applied to the ring electrode while both end-cap electrodes are held at earth ground. The RF potential consists of a variable amplitude, V, and a constant angular frequency, Ω. This potential creates a parabolic field inside the ion trap, regularly described as a saddle (Jonscher & Yates, 1996). A representation of this field, generated by the simulation program, SIMION, is

shown in Figure 2-2 This dynamic field repeatedly changes polarity and focuses trapped ions towards the center of the trap The trapped ions travel in an oscillating flight path that can be described by a second-order linear differential equation that was originally solved by Mathieu in order to describe the motion of vibrating drum heads (Mathieu 1868)

The Mathieu equation predicts whether an ion will be stable or unstable within the trap and is represented by the two reduced parameter equations shown below

$$a_z = -2a_r = -16eU/m\Omega^2(r_o^2 + 2z_o^2) \qquad \text{EQ 2-2}$$

$$q_z = -2q_r = 8eV/m\Omega^2(r_o^2 + 2z_o^2) \qquad \text{EQ 2-3}$$

In the previous equations, r_o is the radius of the ring electrode, z_o is the distance from the center of the trap to the end-cap, e is the charge of an electron (1 602 x 10^{-19} C) U is the DC voltage V is the AC voltage (0 to peak) m is the mass of the ion (kg) and Ω is the angular drive frequency Using these two equations an ion of particular mass can be given coordinates in a_z and q_z space

If the reduced parameters a_z and q_z are plotted together the resulting graph predicts conditions in which an ion of particular mass would be stable within the ion trap The plot known as the Mathieu stability diagram is shown in Figure 2-3 Because the electric fields in the ion trap are uncoupled an ion can be stable in one direction but not in the other For example if an ion is unstable in the r-direction it will oscillate away from the center of the trap and strike the ring electrode just as an ion unstable in the z-direction will oscillate towards the end-cap electrodes However an ion stable in both directions will be trapped

and will oscillate around the center of the trap with a trajectory that closely resembles a Lissajous curve shown in Figure 2-4 (Wuerker *et al.*, 1959).

An ion oscillates inside the trap at its secular frequencies in the axial and radial directions (ω_z and ω_r respectively). These are the frequencies at which an ion travels a complete path in the z and r directions within the trap and are related to the angular frequency (Ω), which is applied to the ring electrode, by Equation 2-4.

$$\omega_u = \beta_u \Omega/2 \quad \text{(where u equals r or z)} \qquad \text{EQ 2-4}$$

Therefore, an ion at a given q_z and a_z, which are related to β_z in the stability diagram, will have a particular secular frequency regardless of the ion's m/z. At the right-hand ejection boundary of the stability diagram, an ion will have β_z=1 and thus a secular frequency (ω_z) exactly half the drive frequency (Ω).

Although there are other stable regions, the most commonly used region of the stability diagram is the one near the origin in Figure 3 and can be seen in detail in Figure 2-5. This region of stability has boundaries from β_z or β_r = 0 to β_z or β_r = 1 with β_z and β_r being iso-beta lines. The β_z = 1 line intersects with the q axis at q = 0.908, which defines the mass range of ions that can be trapped. Since no DC voltage is added on the ring electrode in the experiments to be described here, a_z in Equation 2-2 above will equal zero and ions will therefore reside along the a_z = 0 line (x-axis). Ions line up on the a_z = 0 line with high mass ions at low q_z values and low mass ions at high q_z values, as described in Equation 2-3. The amplitude of the RF voltage governs the lowest m/z that will have a stable trajectory in the trap, known as the low mass cut-off (LMCO). The

ion at the LMCO is sitting on the right hand boundary of the stability diagram Any ion with a lower m/z will sit to its right in the diagram and will not be stable in the trap

The parameter q_z is the most important parameter in determining the position of an ion within the stability diagram at any moment during analysis By knowing the m/z of the ion sitting at the LMCO and the q_z at the far right hand edge of the stability diagram known as the q_z of ejection (q_z = 0 908) the q_z of any other ion can be determined by Equation 2-5

$$m_1q_1 = m_2q_2 \qquad \text{EQ 2-5}$$

where m_1 and q_1 is the m/z and q_z of the ion of interest m_2 is the LMCO and q_2 is the q_z of ejection

Finally the effect of the trapping field is not constant at all q_z values and it takes more or less kinetic energy to eject ions from the trap depending on their position in q-space The ability of an ion to withstand the forces placed on it by the trapping field is governed by the potential well depth and is determined by Equation 2-6 for q_z values less than 0 4 (Major & Dehmelt 1968)

$$D_u = mq_z^2\Omega^2u_o^2/16e \qquad \text{EQ 2-6}$$

From this equation it is shown that ions located at a higher q_z will be in a deeper potential well and will therefore require more energy to excite or eject them whereas ions located at lower q_z are in a shallower potential well and require less energy to excite them For values of q_z greater than 0 4 the calculation for potential well depth is significantly more complicated (March 1995) However

this equation provides sufficient information for the brief overview of the ion trap in this discussion

Obtaining a Mass Spectrum

In order to acquire a mass spectrum, a series of steps must take place within the ion trap mass spectrometer. First, the analyte must be ionized and the ions directed into the trap. This step can be accomplished in a number of ways, as will be discussed at greater length later in this chapter. Once the ions reach the trap, they must be injected into the ion trap and be trapped by the fields associated with the device. Finally, the ions must be mass-selectively ejected from the trap and detected.

In the first ion trap instruments, ions were formed within the trap by internal electron ionization (EI). This was accomplished by introducing a gaseous sample into the trap volume. Electrons from a filament were then brought into the trap to collide with analyte molecules, creating analyte ions (Chapman, 1994). However, the introduction of sample molecules into the trap volume for internal ionization increases the likelihood of further ion-molecule reactions, which can lead to unwanted ions being produced.

To overcome this problem, ions can be generated in a source external to the ion trap and injected into the trap. This allows for control of the number of ions within the trap, which improves resolution, sensitivity and mass accuracy (Stafford *et al.*, 1987). A major consideration when injecting ions into an ion trap concerns the kinetic energy barrier at the entrance of the ion trap (Quarmby & Yost, 1999). An ion must have enough kinetic energy to overcome this barrier

created by the RF potential on the ring electrode in order to enter the ion trap. Conversely, an ion with too much kinetic energy will pass through the trap without enough trapping energy to stop it. By adding a buffer gas, typically helium at 1 mtorr, inside the ion trap, ions accelerated from an external source can be collisionelly cooled and subsequently trapped (March, 1997).

Once the ion trap is filled, ions must be ejected from the trap in order to be detected. The most common technique for ion ejection from an ion trap is the "mass selective instability" scan developed by Stafford in 1985 (Stafford *et al.*, 1985). A mass selective instability scan uses no DC potential so the ions line up on the $a_z = 0$ line in the stability diagram, as mentioned earlier. To eject ions, the amplitude of the RF potential applied to the ring electrode is ramped, causing the ion's q_z value to increase. When the ion's q_z value reaches $q_z = 0.908$, the ion becomes unstable in the z-direction and is ejected through one of the end cap electrodes. If the ion is ejected out of the exit end-cap electrode, it will strike the dynode and be detected by the electron multiplier.

Ejection at the right-hand edge of the stability diagram can result in poor resolution and peak shape (Stafford *et al.*, 1985). By adding a supplementary alternating current (AC) potential across the end-caps at the secular frequency of the ions slightly before the right-hand edge of the stability diagram, the peak shape and resolution is greatly improved (Tucker *et al.*, 1988). This AC potential, called resonant ejection amplitude, causes ions to move from the center of the trap toward the end-cap in a tight packet. This method of ion ejection is called resonant ejection or axial modulation (Stafford *et al.*, 1985).

Tandem Mass Spectrometry

Tandem mass spectrometry (MS/MS) is a popular technique due to the sensitivity and selectivity of two consecutive stages of mass spectrometry (Yost & Fetterolf 1983). Most early MS/MS experiments were performed on triple quadrupole mass spectrometers or multiple sector instruments. These instruments can be described as tandem-in-space instruments because ions move through different stages of the spectrometer during the MS/MS experiment (Yost & Boyd 1990). The QIT is also capable of performing MS/MS experiments, but is considered a tandem-in-time instrument because ions remain within the trap throughout the experiment (Johnson *et al.*, 1990). Because the stages of MS are performed sequentially, with the ions staying in one place, the QIT has a greater MS/MS efficiency, which can lead to improved sensitivity over tandem-in-space instruments.

The process for initially filling the ion trap and scanning the ions out of the trap is the same as described above. However, two new steps must be added to generate a MS/MS spectrum. First, once the trap is filled, the ion of interest must be isolated from the rest of the ions in the trap. This ion is called the parent or precursor, ion. There are many methods for isolating the parent ion but the most common method is by applying a broadband waveform that ejects all ions from the trap except for the parent ion (Bier & Schwartz, 1997).

Once the parent ion is isolated, it can be fragmented by collision-induced dissociation (CID) (Louris *et al.*, 1987). With CID, the parent ion is excited by the application of a dipolar AC signal 180° out of phase and at the ion's secular

frequency across the end-cap electrodes. This method is called resonant excitation. The frequency corresponds to the ω_z of an ion at a specific q_z value. Therefore, the parent ion is moved to the q of excitation before the resonant excitation waveform is applied. When the parent ion is excited, it gains kinetic energy and begins to oscillate across a larger path but not enough to be ejected. This increased flight path brings the parent ion into contact with the buffer gas in the ion trap in a series of collisions. These collisions impart internal energy into the parent ion, causing fragmentation of the parent ion. The resulting fragment ions are called daughter or product ions and can be scanned out of the ion trap and detected by the multiplier as described above.

Laser Desorption Ionization

Laser desorption (LD) ionization techniques are an effective way to produce ions to be analyzed by mass spectrometry. Shortly after the laser was invented in the early 1960s, it was shown that ions are produced from the rapid heating of a solid sample by the application of a focused laser beam (O'Shea *et al.* 1976). When a laser beam ($10^6 - 10^8$ W/cm^2) is focused onto a biological sample, a wide range of thermally labile and non-volatile compounds can be vaporized and ionized (Hercules *et al.*, 1987). Furthermore, LD has the advantage over other desorption ionization techniques, such as fast atom bombardment (FAB) and secondary ion mass spectrometry (SIMS), of probing through the surface and into the secondary layers of the sample (Kelland & Wellach, 1987). As mentioned earlier, one of the biggest advantages of LD techniques over other techniques is the limited sample preparation required and

the elimination of the need for chromatographic separation. Thus, LDMS provides a sensitive and selective method for analyzing biological samples without much sample clean up and/or analyte derivatization (Lee & Yost, 1988).

The first reported application of LDMS was for the elemental analyses of metal surfaces with a pulsed ruby laser in 1963 (Honig & Woolston, 1963). At present, LD has been coupled to a variety of mass analyzers, including sector (Bingham & Salter, 1978), quadrupole (Perchalski *et al.*, 1983), time-of-flight (Spengler & Cotter, 1990) and ion trap (Schwartz & Bier, 1993; Varges, 1993; Reddick, 1997; Troendle, 2000) mass spectrometers. It is difficult to use a quadrupole or sector instrument coupled to an LD source because laser desorption is a pulsed ionization event and the quadrupole and sector are continuous mass analyzers. However, the ion trap is a good fit with LD ionization because both are pulsed techniques.

The first reported use of LD ionization on an ion trap mass spectrometer was by Cotter in 1989 (Cotter *et al.*, 1989). In that study, sucrose and leucine enkephalin were analyzed by internal ionization. This was accomplished by drilling two holes in opposite sides of the ring electrode so that the laser could be focused onto a sample plate brought in through the second hole, within the ion trap. The first reported injection of ions formed in an external source by LD and injected into an ion trap was for the analysis of gold by Louris, also in 1989 (Louris *et al.*, 1989).

Presently, LDMS is not routinely performed on samples from biological matrices because many biomolecules undergo thermal degradation at the high

laser powers required for ionization (Cotter & Tabet 1984). This is due to both resonant and non-resonant desorption of the analyte (Karas *et al.* 1991). With resonant desorption, the direct excitation of the analyte channels energy into vibrational modes, leading to photodissociation. With non-resonant desorption the high laser powers used generate a plasma at the sample surface, leading to molecular degradation. Either way, the use of LD ionization degrades the biological sample and is therefore unfit for analysis by mass spectrometry (McCrery & Gross, 1985).

Matrix-Assisted Laser Desorption Ionization

In response to the degradation of biological analytes by LDMS, it was found that the addition of a matrix to the biological sample increased the production of intact molecular ion species. In 1988, Tanaka detected lysozyme (MW 14,306), from a chicken egg white, in a matrix of ultra fine cobalt powder in glycerol (Tanaka *et al.*, 1988). Upon irradiation from a nitrogen laser (λ = 337 nm), the cobalt powder absorbed the power from the laser light, which, in turn, heated the glycerol and ionized the lysozyme.

At the same time, Karas and Hillenkamp noticed that different amino acids exhibited different absorbances at the wavelength of a frequency tripled Nd:YAG laser (λ = 355 nm) (Karas & Hillenkamp, 1988). Furthermore, it was observed that amino acids with a larger absorbance at the laser's wavelength required less laser power in order to be ionized than amino acids with a smaller absorbance. However, when a mixture of tryptophan, a strongly absorbing amino acid, and alanine, a weakly absorbing amino acid, was analyzed by the laser, $[M+H]^+$ ions

of both amino acids were observed at laser powers well below that required to ionize alanine alone. Based on this experiment, another highly UV absorbing compound, nicotinic acid, was mixed with bovine albumin (MW 67 000) for analysis by time of flight mass spectrometry (TOF-MS). A drop of the mixture was placed on a probe tip and was ionized by a frequency quadrupled Nd:YAG laser (λ = 266 nm). As expected, the resulting spectra consisted of bovine albumin's $[M+H]^+$ ion. Although the two groups published their results at the same time, Karas and Hillenkamp are generally recognized as the originators of MALDI. Despite this common perception, Tanaka was awarded a portion of the Nobel Prize for Chemistry in 2002 for his role in the development of MALDI.

As Karas and Hillenkamp demonstrated with their experiment, a major role of the organic matrix in MALDI is the absorption of the UV radiation. This causes rapid, localized heating of the matrix and analyte, which leads to rapid evaporation of the mixture. This process, shown in Figure 2-6, is described in detail by the "hydrodynamic model" of the desorption process proposed by Vertes (Vertes *et al.*, 1993).

MALDI generally produces ions from biomolecules with little or no fragmentation. However, matrix ions are produced with significant fragmentation. This observation is explained by the "homogeneous bottleneck" model of desorption (Vertes *et al.*, 1990). This model suggests that energy pathways of the matrix-analyte system prefer the formation of intact analyte ions due to the efficient transfer of internal energy between the analyte and excess of matrix.

Further roles of the organic matrix in MALDI include spatial separation of analyte molecules and proton donation to the analyte. The large excess in which the matrix is applied achieves separation of analyte molecules from one another. This allows the majority of the laser energy to be absorbed by the matrix, leaving the analyte intact. Proton donation from the matrix to the analyte is also important to the ionization process, which is indicative of the fact that most MALDI matrices are acids (Zenobi & Knochenmuss, 1998).

Although the desorption process in MALDI is understood, the ionization process is still debated. One thing that is generally accepted is the idea that the ionization process for MALDI is not a single one, but a collection of processes (Spengler *et al.*, 1987). Some of these processes are described briefly below.

The two main categories of ion formation can be termed primary and secondary ion formation (Zenobi & Knochenmuss, 1998). Primary ion formation covers pre-formed ions (ions in the condensed phase) and those ions produced by the initial desorption event. Primary ionization generally involves the formation of matrix ions. Secondary ion formation covers all other ions not generated by primary ionization processes. This generally corresponds to analyte ion formation.

A large number of matrix ions are formed in the condensed phase by solvation in the matrix. When the solid matrix crystals are desorbed, these ions are transferred into the gas phase. In addition to these pre-formed ions, a number of matrix ions are produced by multiphoton ionization mechanisms.

The most common mechanism is shown in Equation 2-7 where M represents a matrix molecule and e represents an ejected electron

$$M + n(h\nu) \rightarrow M^{+} + e \qquad \text{EQ 2-7}$$

This mechanism is consistent with the model that MALDI is dependent on the UV absorbance of the matrix Furthermore additional matrix ions can be produced during collisions with electronically excited matrix molecules during plume expansion

Since the plume formed during desorption is dense, many molecule-molecule and ion-molecule collisions occur Furthermore, hydrogen atoms are found in significant quantities within the plume (Scott *et al* , 1994) This leads to $(M + H)^{+}$ ion formation of the analyte as a result of gas-phase proton transfer

The first report of MALDI coupled to an ion trap was made by Cotter in 1992 (Cotter *et al* 1992) Using the same instrument described in the LDMS section above a mixture of angiotensin I, α-endorphin and parathyroid hormone was analyzed after being mixed with matrix on a probe tip and inserted into the trap through the hole in the ring electrode

Following this work, Bier developed the first MALDI QIT instrument using an external ion source (Schwartz & Bier, 1993) This instrument was made from a modified triple quadrupole instrument with a electron ionization (EI) source The three sets of quadrupole rods were removed and replaced with a set of ion trap electrodes In order to focus the laser onto the sample plate holes were drilled into the extraction lenses and the laser radiation was brought into the

source through a fiber optic cable positioned at the holes. Using this design, several peptides and proteins were analyzed.

Laser Microprobe Instrument

All experiments reported in this dissertation have been performed on a laser microprobe-quadrupole ion trap instrument constructed at the University of Florida (Reddick, 1997; Troendle, 2000). A schematic of the instrument is shown in Figure 2-7. The ionization region of the instrument is composed of a Finnigan 4500 EI/CI ion source from Thermo Finnigan (San Jose, CA). A removable aluminum probe tip is fitted into the backside of the ion volume through a probe lock for analysis. This allows for the preparation of sample outside the vacuum chamber and access to the ion volume without breaking vacuum. The ion volume is mounted orthogonal to the mass analyzer region allowing the laser beam to be focused directly onto the sample surface at a 90-degree angle. This also allows the probe tip to be manipulated by an x-y stage mounted on the source flange. A quartz window allows for transmission of the laser beam onto the sample surface. A DC quadrupole placed just after the ion volume turns the ions 90° towards the mass analyzer region. With this design, the plume of desorbed ions is formed perpendicular to the probe tip and in the direction of the extraction and focusing lenses.

The Finnigan 4500 EI/CI source, shown in Figure 2-8, consists of a stainless steel source block containing two flat electrostatic lenses and a tube lens. The ion source is fitted with an EI ion volume and rhenium filament so that the instrument can be mass calibrated by EI analysis of perfluorotributylamine

(PFTBA) brought into the source via a leak valve. The Finnigan 4500 ion volume has been modified by removing the back wall so that the sample tip completes the volume when the probe is inserted into the source.

An aluminum wall divides the vacuum chamber of the instrument allowing for differential pumping of the ionization and mass analysis regions. Each region is pumped by a separate TPH 270 turbomolecular pump (Balzers) which is backed by a 300 L/min mechanical pump (Alcatel). A VSL-337ND pulsed nitrogen laser (Laser Science, Inc.) is used for ionization. The laser operates at 337.1 nm with a spectral bandwidth of 0.2 nm. The laser produces a 3 ns pulse width (FWHM) at a repetition rate of up to 20 Hz. An ITS-40 ion trap, from Thermo Finnigan, is used for mass analysis. The use of an ion trap for the mass analyzer is of importance in this research due to its ability to perform tandem mass spectrometry (MS/MS) on a pulsed packet of ions produced by MALDI. Gatorware, software developed by Tim Griffin, was used to control instrumental parameters for each analysis (Griffin, 1995).

Gatorware operates the Finnigan ITS40 electronics package that powers the instrument. The software allows the user to control the operation of the ion trap through a series of scan tables, shown in Figure 2-9. Each scan table tells the scan and acquisition processor (SAP) electronics board what voltages to apply to the ion trap throughout the scan and for what period of time. Gatorware also provides the user control over the set of voltages for resonant excitation and ejection of ions.

Figure 2-1 Schematic of the quadrupole ion trap (QIT). The QIT is made up of three cylindrically symmetrical electrodes: an entrance end cap, a ring electrode and an exit end-cap. Adapted from Quarmby, 1997.

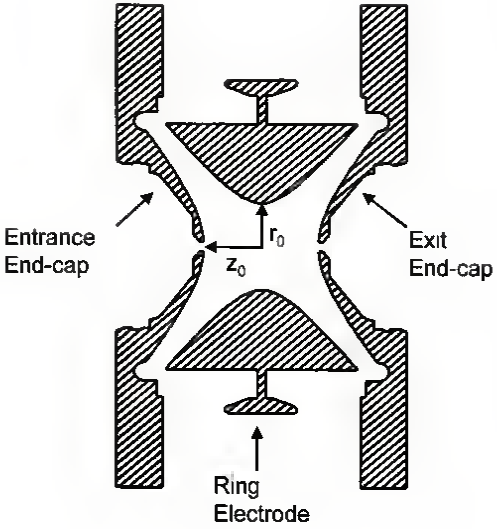
Entrance
End-cap
r_0
z_0
Exit
End-cap
Ring
Electrode

Figure 2-2 Saddle-shaped parabolic field inside the ion trap When a positive potential is placed on the ring electrode positive ions are repelled from the ring electrode and attracted to the end-cap electrodes When the polarity is switched and a negative potential is placed on the ring electrode positive ions are attracted to the ring electrode and repelled from the end-cap electrodes This dynamic field repeatedly changes polarity and focuses trapped ions towards the center of the trap Image adapted from Murphy 2002

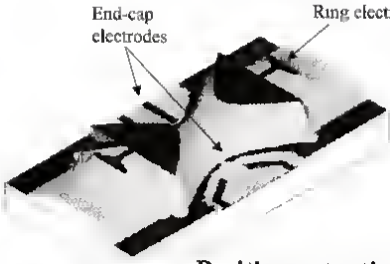

Positive potential on ring electrode

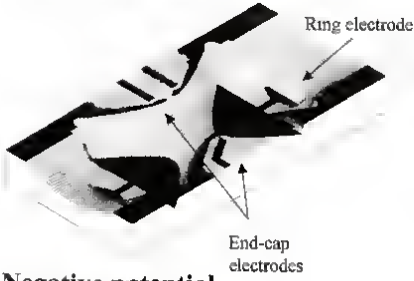

Negative potential on ring electrode

Figure 2-3 Mathieu stability diagram The Mathieu equation predicts regions where an ion will be stable or unstable within the ion trap (Mathieu 1868)

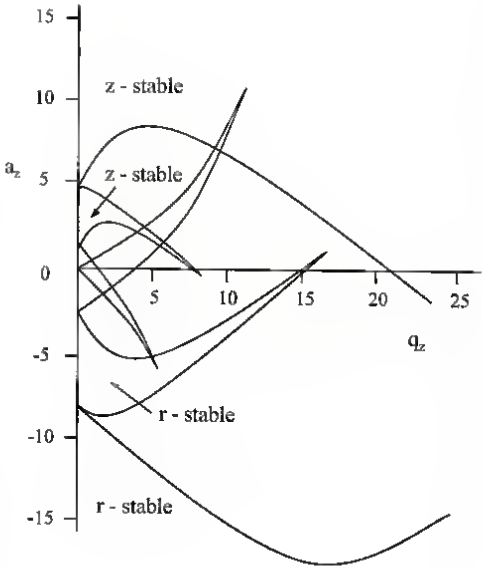
15
10
5
0
-5
-10
-15
a_z
z - stable
z - stable
r - stable
r - stable
5
10
15
20
25
q_z

Figure 2-4 Lissajous Curve. An ion stable in both the r- and z-directions of the ion trap will be trapped and will oscillate in a path shown here. In this image, stable charge aluminum microparticles oscillate in a stable trajectory within an ion trap. Reproduced from Wuerker, 1959

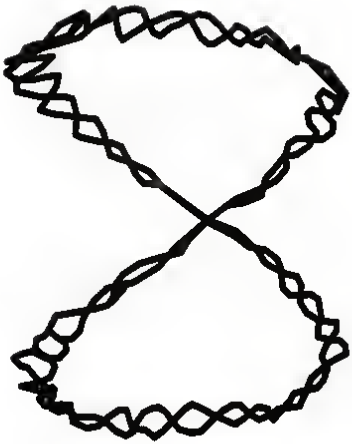

Figure 2-5 Most used region of the Mathieu stability diagram This region of stability has boundaries from β_z and $\beta_r = 0$ to β_z and $\beta_r = 1$ with β_z and β_r being iso-beta lines The $\beta_z = 1$ line intersects with the q axis at q = 0 908 which defines the mass range of ions that can be trapped at $a_z = 0$

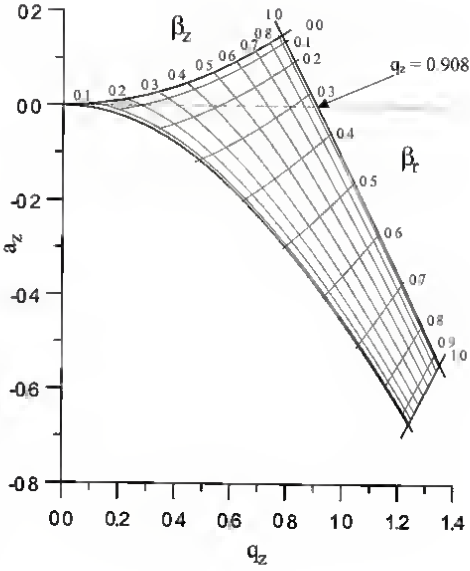
02
00
-02
-04
-06
-08
a_z
00
0.2
0.4
0.6
0.8
1.0
1.2
1.4
q_z
β_z
β_t
$q_z = 0.908$
0.1
0.2
0.3
0.4
0.5
0.6
0.7
0.8
0.9
1.0

Figure 2-6 **MALDI mechanism** A major role of the organic matrix in MALDI is the absorption of the UV radiation. This causes rapid, localized heating of the matrix and analyte, which leads to rapid evaporation of the mixture.

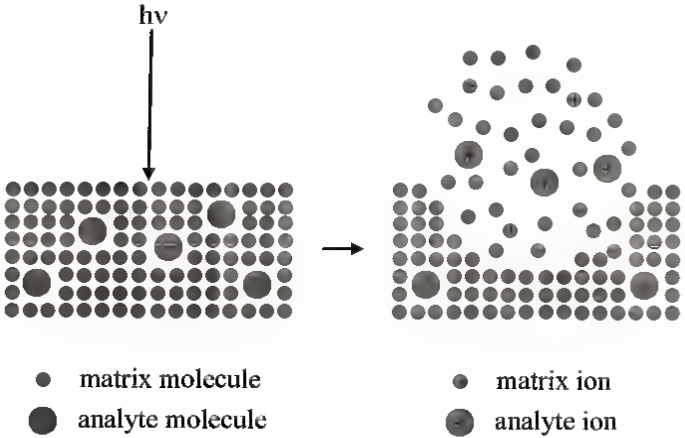
hν
matrix molecule
analyte molecule
matrix ion
analyte ion

Figure 2-7 Laser microprobe mass spectrometer. This quadrupole ion trap mass spectrometer was used for analyses described in this dissertation.

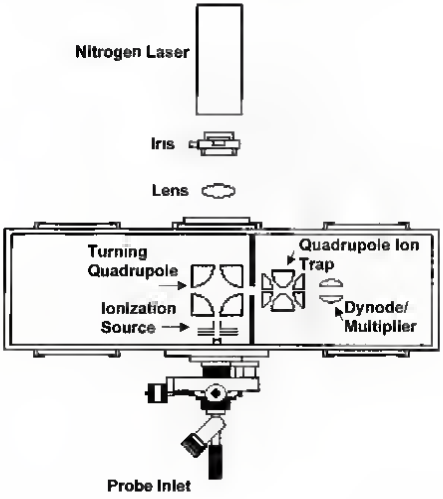
Nitrogen Laser
Iris
Lens
Turning
Quadrupole
Ionization
Source
Quadrupole Ion
Trap
Dynode/
Multiplier
Probe Inlet

Figure 2-8 Laser microprobe mass spectrometer ionization source The Thermo Finnigan 4500 EI/CI source consists of a stainless steel source block containing two flat electrostatic lenses and a tube lens The ion source is fitted with an EI ion volume and rhenium filament so that the instrument can be mass calibrated by EI analysis of perfluorotnbutylamine (PFTBA) brought into the source via a leak valve

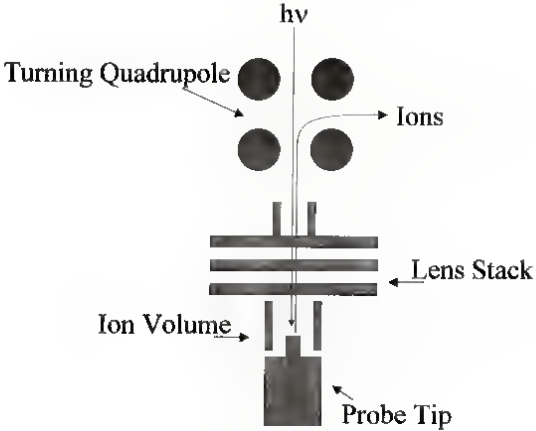
hν
Turning Quadrupole
Ions
Lens Stack
Ion Volume
Probe Tip

Figure 2-9. Gatorware scan table. Gatorware operates the Finnigan ITS40 electronics package that powers the instrument. The software allows the user to control the operation of the ion trap through a series of scan tables. Each scan table tells the scan and acquisition processor (SAP) electronics board what voltages to apply to the ion trap throughout the scan and for what period of time.


Control
Options
File
Table
Exit
100x = 1000
TIC 0
Tonix 3000 usec
C:\MSMS-40\SCAN\TUNE SCH
50
100
150
200
250
300
350
400
450
500
550
600
TABLE: 3 IONIZE
0Tables: 7
Auto Down. on
Table Calc. on
Mult
Scan
Fil
Togl
RF
Time (us)
3000
Table Mass
396.0
Freq (Hz)
0
Start az
0.00220
Start qz
0.067
Ampl (mV)
0
End az
0.00220
End qz
0.067
Phase(deg)
0
CI
MULT
1700
TTL1
TTL2
TTL3
FREQ
AMPL
WAIT
Tables
Acquire
Cal
Rate

CHAPTER 3
CARNITINE ANALYSIS BY LDMS TECHNIQUES

Carnitine Structure

L-carnitine and its fatty-acid derivatives ,structures shown in Figure 3-1 share a free carnitine backbone and therefore exhibit similar fragmentation patterns For example all acylcarnitines exhibit a neutral loss of 161 amu due to the loss of the free carnitine backbone Also carnitines carry a positive charge at their trimethylamino group and therefore commonly exhibit a neutral loss of 59 amu upon MS/MS analysis The daughter ion produced by this loss is generally the most intense ion in the MS/MS spectrum for l-carnitine and its derivatives Furthermore carnitines often produce a fragment ion at m/z 60 attributed to the trimethylammo functionality plus a proton Finally carnitines give a characteristic daughter ion at m/z 85 This fragment corresponds to the loss of both the fatty acid group and trimetylamino functionality leaving the $^{+}CH_2CH{=}CHCOOH$ ion Table 3-1 lists the expected fragment ions for l-carnitine and a number of acylcarnitines

MALDI Sample Preparation

The organic matrix 2 5-dihydroxybenzoic acid (DHB) was used for the MALDI analyses of acylcarnitines in this research Another matrix α-cyano-4-hydroxycinnamic acid (CHCA) was originally used but the chemical background signature of the matrix was too complex at low m/z values and

interfered with the acylcarnitine ions produced in that region. Both matrices were purchased from Sigma-Aldrich.

Although DHB is a relatively simple matrix, it does produce characteristic fragment and adduct ions that can interfere with analytes of low m/z. The two most intense background ions for DHB (MW = 154 Da) are at m/z 137 and m/z 273. These ions are shown in the mass spectrum of a DHB sample in Figure 3-2 along with the structure of DHB. The ion at m/z 137 corresponds to the protonated molecular ion of DHB minus water, $[M + H - H_2O]^+$, and the ion at m/z corresponds to the protonated DHB dimmer minus two waters, $[2M + H - 2H_2O]^+$. Other ions present in the background spectrum correspond to matrix fragments and other impurities in the matrix solution. These matrix background ions are significantly less hindering than those produced by CHCA for the analysis of low molecular weight compounds, yet are still quite intense and often dominate the spectrum in the low m/z region.

The matrix was prepared as a saturated solution by first adding a small amount of solid DHB into an Eppendorf tube. Methanol was added to the tube and the mixture was vortexed for thirty seconds. After vortexing, the mixture was centrifuged for five minutes. The supernatant was then poured into a fresh Eppendorf tube and used as the matrix solution for MALDI analysis.

Carnitine Analysis

For carnitine analysis, sample solutions of l-carnitine and a number of acylcarnitines were prepared. L-carnitine and the acylcarnitines propionyl-, isobutryl-, isovaleryl- and octanoylcarnitine were purchased from Sigma. Stock

solutions (3 mM) for each of these compounds were prepared in 1:1 methanol/chloroform and all subsequent dilutions were made with 1:1 methanol/chloroform as well.

To prepare for analysis, one microliter of the acylcarnitine solution was pipetted onto the probe tip and dried under a stream of air. Once dry, one microliter of the DHB matrix solution was added to the probe tip and was allowed to dry. The probe tip was then mounted onto the probe and inserted into the source of the mass spectrometer through the vacuum lock.

A mixture of l-carnitine, propionylcarnitine, isobutyrylcarnitine, isovalerylcarnitine and octanoylcarnitine was prepared on the probe tip in the fashion mentioned above and the corresponding full scan mass spectrum is shown in Figure 3-3. The solution was prepared so that 50 ng of each compound was deposited onto the probe. In this full scan spectrum, the $[M + H]^+$ ions for each of the carnitines are present at m/z 162, m/z 218, m/z 232, m/z 246 and m/z 288 corresponding to l-carnitine, propionylcarnitine, isobutyrylcarnitine, isovalerylcarnitine and octanoylcarnitine, respectively. Note also the presence of the DHB background ions mentioned above.

For this study, l-carnitine and octanoylcarnitine were the primary biomarkers for the screening of the metabolic disorder MCADD. Since the two analytes of interest are in the same chemical family, with similar fragmentation patterns, characteristic ions specific to each biomarker needed to be identified in order to choose the characteristic ions for quantitation of these biomarkers. MS/MS spectra were generated for each of the compounds.

To generate a daughter spectrum for l-carnitine the trap was filled with ions produced by MALDI and the $[M + H]^+$ ion for l-carnitine (m/z 162) was moved to a q value of 0 80 using the Gatorware software program Once there the ion was isolated using a stored waveform inverse Fourier transform (SWIFT) waveform for a duration of 100 ms The waveform was designed so that ions within a 10 amu wide isolation window centered around m/z 162 would remain in the trap and all other ions would be ejected Once isolated the parent ion was dropped to a q value of 0 20 before CID was performed This is done so that the daughter ions produced by CID which are of lower m/z than the parent ion will remain stable within the ion trap before the final scan-out event. CID of the parent ion was accomplished by applying a dipolar signal across the end cap electrodes at a frequency of 76 kHz and amplitude of 600 mV for 150 ms

The resulting daughter spectrum is shown in Figure 3-4 Note the presence of the characteristic carnitine ion at m/z 60 and the fragment ion at m/z 103 This latter ion corresponds to the loss of the trimethylamino group (neutral loss of 59 amu) and is the base peak A daughter spectrum for octanoylcarnitine was also generated in the manner explained above with two exceptions. First, the $[M + H]^+$ ion for octanoylcarnitine was isolated (m/z 288) Second an amplitude of 800 mV was used for CID This daughter spectrum is shown in Figure 3-5 Note the presence of the ion at m/z 229 corresponding to the neutral loss of 59 amu as the base peak The peak at m/z 127 corresponds to the loss of the carnitine backbone (neutral loss of 161 amu) and the fragment at m/z 85 described earlier, further confirms the presence of a carnitine-based compound

The characteristic carnitine fragment ion at m/z 60 is not found in this spectrum due to the low mass cut-off inherent to the ion trap instrument

Since the fragment ions corresponding to the neutral loss of 59 amu are the base peaks for both l-carnitine and octanoylcarnitine (m/z 103 and m/z 229 respectively), these characteristic daughter ions were used in the generation of calibration curves for each compound. Solutions were diluted from the stock solutions over a range from 200 ppm to 2 ppb for l-carnitine and 300 ppm to 3 ppb for octanoylcarnitine. This concentration range covered the typical biological levels of 3 ppm to 13 ppm for l-carnitine and 1 ppm to 6 ppm for octanoylcarnitine that were discussed earlier. When the solution was spotted onto the probe tip in one microliter doses, this corresponded to a range of 200 ng to 2 pg deposited for l-carnitine and 300 ng to 3 pg for octanoylcarnitine.

The calibration curves for l-carnitine and octanoylcarnitine, shown in Figure 3-6 and Figure 3-7, consist of five data points from sample concentrations within the range described above. Each data point is the average of three ablation spots. At each ablation spot, five mass spectra were averaged with five microscans making up a mass spectrum. Each microscan consists of three laser pulses. Therefore, each mass spectrum is the average of fifteen laser pulses and each spot is the average of forty-five laser pulses. The error bars represent the standard deviation of the mean.

The presence of large error bars in both calibration curves shows a lack of precision for the direct MALDI calibration of these two compounds. Furthermore, even though extremely accurate quantitation is not required for screening, the

poor fit of the trend lines attributed to the data sets is not at all reliable for quantitative use. Therefore, in order to perform quantitative analysis by LD/MS techniques, the use of internal standards is necessary.

Internal Standard

Quantitation by laser desorption techniques is not a trivial task due to a number of variables, including laser shot-to-shot variance, inhomogeniety of the matrix crystals and surface inconsistencies. For example, Figure 3-8 shows a plot of intensities of the DHB fragment at m/z 137 over a period of ten shots. Each data point in this plot represents one laser pulse followed by an analytical scan. The mean intensity the DHB fragment over the ten laser shots was calculated to be approximately 25 000 units and is represented by the solid line. The standard deviation of the ten data points was calculated to be approximately 10,000 units from the mean and is represented graphically by the dashed lines. This experiment shows that there can be as much as 46% variance in the intensity of an ion between successive laser pulses for MALDI analysis with this particular instrument. In order to overcome this problem, an internal standard was used for all subsequent experiments that required quantitation.

It was important to find an internal standard with an ionization efficiency similar to the acylcarnitine analytes used in this study. This is to insure that both compounds are ionized consistently from laser shot to laser shot. Deuterated analougues of l-carnitine and octanoylcarnitine would be ideal compounds for use as internal standards in this study for a number of reasons. First, they closely resemble the chemical nature of the analyte to be quantitated, and would

therefore be ionized with similar efficiency. Second, their closeness in molecular weight would allow the analyte and internal standard to be isolated easily within the same isolation window. This is important since tandem mass spectrometry is to be used in this study to increase selectivity. Unfortunately, deuterated acylcarnitine standards were not ultimately used in this study due to difficulty in in-house production of the compounds and the high price of purchasing them from outside vendors.

It was therefore determined that the use of a separate acylcarnitine would be a good internal standard since the similarities in chemical structure would yield similar ionization efficiencies. Consequently, isobutyrylcarnitine was chosen as the internal standard for this study. Isobutyrylcarnitine (MW 231 Da) has a molecular weight between those of l-carnitine and octanoylcarninitine and could be therefore used as the standard for each analyte.

To get mass spectral data for both the analyte and internal standard from the same ionization event, the $[M+H]^+$ ion for each must be isolated within the same window. This is accomplished by increasing the frequency range of the SWIFT waveform used for isolation. Once isolated, the analyte parent ion is fragmented by collision-induced dissociation but the $[M+H]^+$ ion of the internal standard is left intact. This results in a mass spectrum with MS/MS data for the analyte along with the intact $[M+H]^+$ peak for the internal standard.

However, any ions formed with a m/z value between the analyte parent ion and the internal standard parent ion will also remain stable within the isolation window and will therefore be kept in the ion trap upon isolation and subsequently

scanned out with the ions of interest in the analytical scan. This includes any organic matrix background ions that are formed within this m/z range. Isolation is generally performed with a relatively narrow isolation window and MALDI matrix ions do not interfere with MS/MS experiments because they are removed upon the isolation of the analyte parent ion. However, in this case, the background interference is similar to that seen in single-stage MALDI-MS experiments and hinders the collection of quantitative data because the isolation window is so wide. Therefore, it was determined that traditional MALDI would not be the ideal method for this analysis due to the chemical background inherent to the organic matrix.

Desorption Ionization on Porous Silicon

Recently, a method for pulsed laser desorption ionization of biomolecules without the use of an organic matrix was described (Wei *et al.*, 1999). For this technique, called desorption ionization on porous silicon (DIOS), the sample is deposited onto a porous silicon surface and analyte ions are produced by a focused ultra violet laser beam illuminating the surface similar to MALDI. However, unlike other matrix free desorption techniques, DIOS typically produces intact molecular ions, in the form of $[M + H]^+$ ions, with little or no degradation of the analyte. Furthermore, since no organic matrix is present in the system, the chemical background that hinders MALDI for the analysis of low m/z compounds is absent. Therefore, when DIOS is coupled to mass spectrometry, the resulting spectra are quite similar to MALDI-MS data without the observation of matrix ions at low m/z values.

Porous silicon is typically produced by electrochemically etching a crystalline silicon wafer in a hydrofluoric acid solution (Canham 1997). Once etched, it has been shown that porous silicon is capable of absorbing ultraviolet radiation (Sailor & Lee 1997). It is believed that the pore system present in the porous silicon surface also retains solvent and analyte and provides spatial separation between analyte molecules (Shen *et al.* 2001). This is possible because porous silicon commonly exhibits large surface areas in excess of 100 m^2/cm^3. The combination of these two qualities allows for solvent and analyte trapped in the pore system to be ionized by transferring laser energy from the porous silicon surface to the analyte.

In this process, the porous silicon surface acts similarly to the organic matrix in MALDI. As mentioned earlier in this text, the organic matrix is responsible for providing spatial separation of analyte molecules, absorbing laser energy and transferring it to the analyte. It is believed that the desorption of solvent, in addition to analyte, aids in providing the protons necessary to produce $[M + H]^+$ analyte ions in DIOS (Kruse *et al.* 2001).

Surface Production

Although the production of porous silicon was first described in the mid 1950's (Uhlir, 1956), there has been a recent increase in research of the surface stemming from Canham's discovery that highly porous silicon emits visible light at room temperature (Canham 1990). This, it is hoped, could lead to a new breed of microprocessors and other optoelectronic devices. Upon further research of the properties of porous silicon, however, it was also discovered that

porous silicon absorbs ultraviolet radiation (Amato & Rosenbauer 1997). Although porous silicon is still primarily researched for optoelectronic uses, this discovery opened the door for its use as an analytical tool with DIOS.

Porous silicon is currently prepared via a number of techniques, including spark source etching (Hummel 1992), laser ablation (Anderson *et al.*, 2002) and electrochemical etching (Cullis *et al.*, 1997). In the first process, a series of unidirectional electric pulses are applied between a tungsten wire, the anode, and a piece of flat crystalline silicon, the cathode. When a potential is applied to the electrodes, the silicon cathode emits electrons that ionize surrounding gas atoms. The bombardment of these ions into the tungsten anode creates enough heat to evaporate portions of the silicon surface. This technique is difficult to control and is quite irreproducible due to the random nature of the spark.

In collaboration with Michael Shepard of the Winefordner group at the University of Florida, the original porous silicon surfaces used in this study were produced by modification of a crystalline wafer using high-energy laser pulses. To do this, one thousand pulses from a XeCl excimer laser (λ = 308 nm) were focused onto a silicon wafer with an energy of 63 mJ per pulse. This resulted in most of the crystalline silicon being ablated, leaving a large hole at the point of incidence on the wafer. However, in the area immediately surrounding the hole, a region of porous silicon was also produced by the partial ablation of the crystalline silicon wafer. A scanning electron micrograph (SEM) of the porous surface is shown in Figure 3-9.

This porous area produced sufficient DIOS signal when analyzed in the mass spectrometer described earlier. However, the presence of the hole in the middle of the useful region made it difficult to deposit sample onto the porous region without unwanted loss through the cavity. This sample loss made it impossible to determine how much sample was actually deposited in the porous region and therefore rendered the porous silicon surfaces produced by laser ablation unfit for the quantitative nature of this study.

Electrochemically etched porous silicon is the most common form of porous silicon and is produced by etching a flat piece of crystalline silicon in a hydrofluoric acid solution in the presence of a constant applied current, and then allowing the silicon substrate to dry by evaporation (Canham, 1997). However, this process can be hampered by the cracking and/or disintegration of the porous system due to capillary tension caused by the liquid-vapour interfaces formed during evaporation of solvent (Amato *et al.*, 1997).

For this study, porous silicon surfaces were ultimately produced using a setup constructed by Mark Villona, of the Winefordner group, in a process illustrated in Figure 3-10. The wafers used were obtained from Silicon Sense and were 525 μm thick, low resistivity (0.02-0.06 ohm*cm), n-type antimony doped silicon. The wafer was first placed on a piece of silver, which acts as the anode in the etching process. The stack was then placed on a copper flag to allow for electrical contact outside the cell and locked into a Teflon cell, which was sealed with o-rings. A 1:1 etching solution of 48% (w/v) HF and ethanol was added to the Teflon well above the wafer surface. A platinum mesh electrode

was submerged in the etching solution so that it sat just above the silicon surface. A constant current density of approximately five microamps was passed through the cell setup from the silver anode to the platinum electrode cathode.

In order to expedite the reaction, white light from a tungsten bulb was focused onto the silicon surface during the etching process. The addition of light to this reaction significantly speeds up the process when n-type silicon is used. However, when using p-type silicon as the precursor, light is not required to facilitate the reaction. This is because the etching process depends on the formation of electron holes, which are inherently present in p-type silicon. However, with n-type silicon, these electron holes must be created. This is accomplished with the energy from the light. It is for this reason that n-type silicon is generally used for the production of porous silicon to be used for DIOS. Since porous silicon will only be produced where electron holes are present, a mask can be used to create an array of modified regions on an n-type wafer. Conversely, if p-type silicon is used, the mask would not be effective and the entire surface would be modified.

After an etching time of approximately two minutes, the silicon sample was removed from the cell, washed in absolute ethanol and dried under a stream of nitrogen. The surface was then placed under a UV lamp to test for room temperature luminescence.

Porous silicon surfaces produced by electrochemical etching are primarily silicon-hydride terminated (Canham, 1997). Although this newly etched surface exhibited room temperature luminescence and was capable of DIOS applications

as is it was not stable and corroded relatively quickly (within three to five days) due to oxidation and the adsorption of impurities in the air. This breakdown of the surface was most evident with use of aqueous samples, which are common in the biological nature of this study. Therefore, if the porous silicon sample surfaces were not to be used immediately, it would be necessary to stabilize them by further reaction.

It has been shown by Buriak et al that porous silicon surfaces can be effectively derivatized with alkyl or alkenyl termination by both white light induced hydrosilation (Stewart & Buriak, 1998) and Lewis acid mediated hydrosilation (Bunek & Allen, 1998). For the white light induced hydrosilation reaction, an appropriate solution of alkyne or alkene is floated over the porous silicon surface. Upon illumination from a tungsten filament, the reaction is rapid, requiring less than sixty minutes for completion. The Lewis acid mediated hydrosilation reaction requires the alkyne or alkene solution to be floated over the porous silicon surface in the presence of ethyl-aluminumdichloride ($EtAlCl_2$). However, for the purposes of this dissertation, the porous silicon surfaces were used immediately after etching and discarded after each use so further derivatization of the surface was not necessary.

Carnitine Analysis

The electrochemically etched porous silicon surface was cut into a 4 mm square by scoring and breaking the wafer. The surface was then attached to the probe tip by a piece of double-sided tape. The probe was then inserted into the mass spectrometer and a background spectrum, shown in Figure 3-11, was

acquired of the bare porous silicon surface. Note that no appreciable chemical background is present in the blank spectrum, unlike the typical background spectrum of MALDI with an organic matrix.

A standard solution of l-carnitine, isobutyrylcarnitine and octanoylcarnitine was prepared in 1:1 methanol/chloroform. One microliter of the analyte solution was pipetted onto the porous silicon surface and dried under a light stream of air. The full scan mass spectrum, shown in Figure 3-12, shows the $[M + H]^+$ ions (at m/z 162, m/z 232 and m/z 288 for l-carnitine, isobutyrylcarnitine and octanoylcarnitine respectively) for each carnitine. Note that, as with the sample blank spectrum, there is a lack of chemical background generated and that there is no fragmentation of the analytes.

In order to construct a set of calibration curves for l-carnitine and octanoylcarnitine, a series of standards were prepared by dilution from the standard solutions. The samples ranged from 100 pg to 100 ng of l-carnitine and octanoylcarnitine deposited on the probe tip. Each sample also contained 28 ng of isobutyrylcarnitine as the internal standard. As mentioned earlier, the SWIFT isolation window was opened wide enough so that the $[M + H]^+$ ion of the isobutyrylcarnitine internal standard could be isolated along with the $[M + H]^+$ ion of either l-carnitine or octanoylcarnitine.

Once isolated, only the $[M+H]^+$ ion ions of the analyte and internal standard were present due to the characteristic limited chemical background of DIOS. CID of l-carnitine was performed in the presence of the internal standard and the resulting mass spectrum is shown in Figure 3-13. Note the presence of

the characteristic l-carnitine fragment ion at m/z 103 and the internal standard $[M+H]^+$ ion at m/z 232. For the standard at each concentration, spectra were taken and a calibration plot was constructed by plotting the ratio of ion intensities for m/z 103 and m/z 232 versus the ratio of the masses of the samples deposited on the probe tip. The calibration curve is shown in Figure 3-14.

Similarly, for the analysis of octanoylcarnitine, the SWIFT isolation window was opened so that both the octanoylcarnitine and isobutyrylcarnitine $[M+H]^+$ ions were present. Upon CID of the octanoylcarnitine parent ion at m/z 288, a fragment ion at m/z 229 was produced and scanned out of the trap along with the internal standard ion at m/z 232. This spectrum is shown in Figure 3-15. By plotting the ratios of these ions in the manner described earlier for the l-carnitine plot, a calibration curve for octanoylcarnitine was produced and is shown in Figure 3-16.

For the calibration curves, each data point represents the average of three laser spots on the probe tip. Each spot is the average of three mass spectra with each mass spectrum made up of five microscans. Each microscan consists of three laser pulses. Therefore, each mass spectrum is the average of fifteen laser pulses and each spot is the average of forty-five laser pulses. The error bars represent the standard deviation of the mean for each data point.

To test the calibration curves effectiveness at predicting the concentrations of an unknown sample during the screening process, three test samples of l-carnitine and octanoylcarnitine were made up over a range of physiological concentrations. Isobutrylcarnitine was added to each solution and

the samples were analyzed in the fashion discussed above For each test sample the concentration extrapolated from the curve was within ten percent of the known concentration of the solution for both analytes

By using an internal standard calibration precision is dramatically increased versus the indirect calibration employed in the MALDI-MS study This is illustrated by the decrease in the error bars over the MALDI method Furthermore the trend line for each data set is sufficient for the rapid estimation of biomarker concentration necessary for screening This is shown by the close correlation of the extrapolated concentration versus the known concentration of the prepared test samples

Drawbacks with DIOS Method

A major drawback to the DIOS technique is based in the production of the porous silicon surface As mentioned earlier, the surfaces produced by laser modification were irreproducible due to inconsistencies in the laser pulse and the ablation of a large hole in the center of the porous region Unfortunately the production of porous silicon surfaces was not completely reproducible using electrochemical etching either This is partly due to differences in the production of the precursor crystalline silicon wafers leading to small differences in the etching process for each batch of sample surfaces More importantly irreproducibility of the sample surfaces stems from the partial collapse of the pore system during the drying of the surface This is due to the capillary forces generated at the liquid-vapour interface during drying and can lead to inconsistent porous surfaces

Table 3-1 Characteristic fragment ions for acylcarnitines

R-group	MW	$[M + H]^+$	$[M - 59]^+$	$[M - 161]^+$
Acetyl	203	204	145	43
Propionyl	217	218	159	57
Isobutryl	231	232	173	71
Isovaleryl	245	246	187	85
Methyl butryl	245	246	187	85
Hexanoyl	259	260	201	99
Octanoyl	287	288	229	127
Lauroyl	343	344	285	183
Myristoyl	371	372	313	211
Palmitoyl	399	400	341	239

Figure 3-1 Acylcarnitine structures. All acylcarnitines share a free carnitine backbone and therefore exhibit similar fragmentation patterns

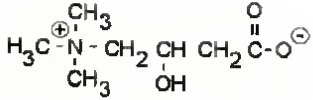

L-carnitine (MW 161)

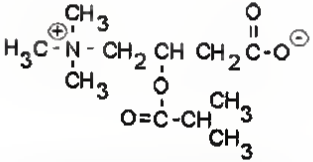

Isobutrylcarnitine (MW 231)

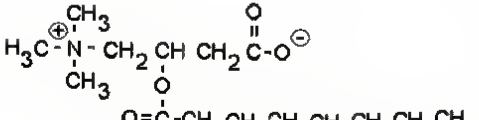

Octanoylcarnitine (MW 287)

Figure 3-2 DHB background mass spectrum. Although DHB is a relatively simple matrix, it does produce characteristic fragment and adduct ions that can interfere with analytes of low m/z. The two most intense background ions for DHB are at m/z 137 and m/z 273. The ion at m/z 137 corresponds to the protonated molecular ion of DHB minus water, $[M + H - H_2O]^+$, and the ion at m/z corresponds to the protonated DHB dimmer minus two waters, $[2M + H - 2H_2O]^+$. Other ions present in the background spectrum correspond to matrix fragments and other impurities in the matrix solution.

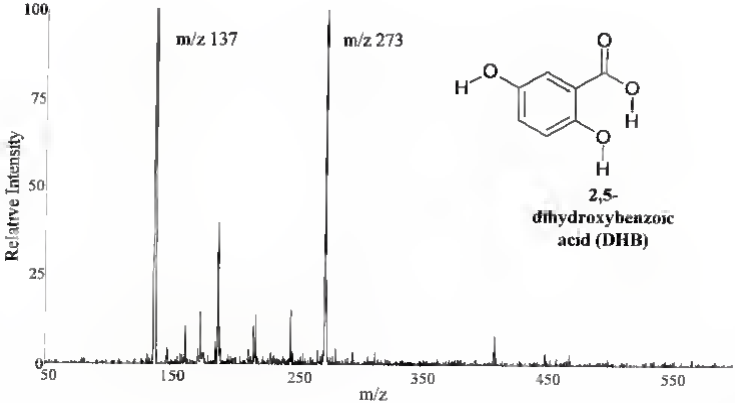
100
75
50
25
0
Relative Intensity
m/z 137
m/z 273
50
150
250
350
450
550
m/z
O
H
O
O
H
O
H
2,5-
dihydroxybenzoic
acid (DHB)

Figure 3-3 MALDI mass spectrum of a mixture of carnitines A mixture of l-carnitine propionylcarnitine isobutrylcarnitine isovalerylcarnitine and octanoylcarnitine was prepared so that 50 ng of each compound was deposited onto the probe In this full scan spectrum the $[M + H]^+$ ions for each of the carnitines are shown at m/z 162 for l-carnitine m/z 218 for propionylcarnitine m/z 232 for isobutrylcarnitine m/z 246 for isovalerylcarnitine and m/z 288 for octanoylcarnitine Note also the presence of the DHB background ions mentioned above

Relative Intensity
100
75
50
25
0
50
100
150
200
250
300
350
m/z
137
l-carnitine
60
85
103
162
propionylcarnitine
173
isobutyrylcarnitine
218
232
isovalerylcarnitine
246
273
octanoylcarnitine
288

Figure 3-4 Daughter spectrum for CID l-carnitine parent ion (m/z 162). Note the presence of the characteristic carnitine ion at m/z 60 and the fragment ion at m/z 103. This latter ion corresponds to the loss of the trimethylamino group and is the base peak.

m/z 103
m/z 85
m/z 60
Relative Intensity
m/z
100
75
50
25
0
50
75
100
125
150
175
200

Figure 3-5 Daughter spectrum for CID octanoylcarnitine parent ion (m/z 288). Note the presence of the ion at m/z 229 corresponding to the neutral loss of 59 amu as the base peak. The peak at m/z 127 corresponds to the loss of the carnitine backbone (neutral loss of 161 amu) and the fragment at m/z 85 further confirms the presence of a carnitine-based compound. The characteristic carnitine fragment ion at m/z 60 is not found in this spectrum due to the low mass cut-off inherent to the ion trap instrument.

m/z 229
m/z 85
m/z 127
Relative Intensity
m/z
100
75
50
25
0
50
100
150
200
250
300

Figure 3-6 L-carnitine calibration curve by MALDI The calibration curve consists of five data points from sample concentrations bracketing the biological range of L-carnitine Each data point is the average of three ablation spots At each ablation spot five mass spectra were averaged with five microscans making up a mass spectrum Each microscan consists of three laser pulses Therefore each mass spectrum is the average of fifteen laser pulses and each spot is the average of forty five laser pulses The error bars represent the standard deviation of the mean

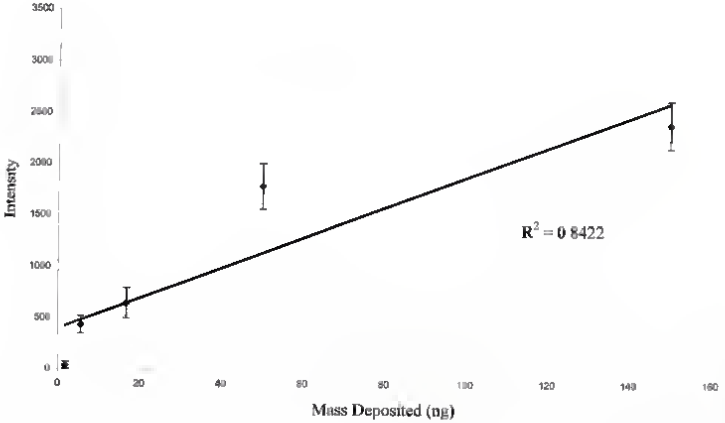
3500
3000
2500
2000
1500
1000
500
0
Intensity
$R^2 = 0.8422$
0
20
40
60
80
100
120
140
160
Mass Deposited (ng)

Figure 3-7 Octanoylcarnitine calibration curve by MALDI The calibration curve consists of five data points from sample concentrations bracketing the biological range of octanoylcarnitine Each data point is the average of three ablation spots At each ablation spot five mass spectra were averaged with five microscans making up a mass spectrum Each microscan consists of three laser pulses Therefore each mass spectrum is the average of fifteen laser pulses and each spot is the average of forty five laser pulses The error bars represent the standard deviation of the mean

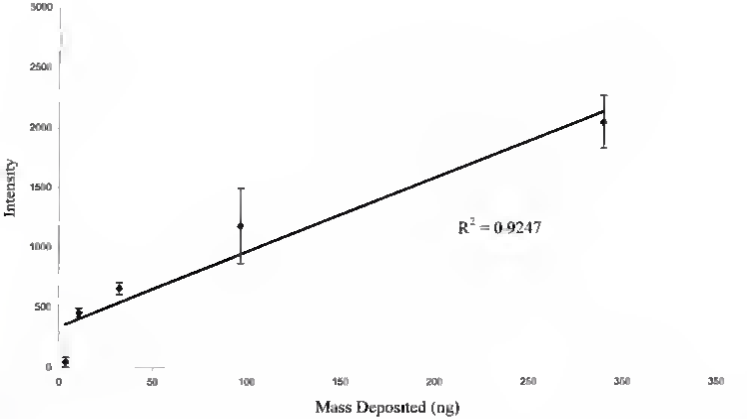
3000
2500
2000
1500
1000
500
0
Intensity
$R^2 = 0.9247$
0
50
100
150
200
250
300
350
Mass Deposited (ng)

Figure 3-6 Shot to-shot variance. This is a plot of intensities of the DHB fragment at m/z 137 over a period of ten shots. Each data point in this plot represents one laser pulse followed by an analytical scan. The mean intensity the DHB fragment over the ten laser shots was calculated to be approximately 25 000 units and is represented by the solid line. The standard deviation of the ten data points was calculated to be approximately 10,000 units from the mean and is represented graphically by the dashed lines. This experiment shows that there can be as much as 46% variance in the intensity of an ion between successive laser pulses for MALDI analysis with this particular instrument.

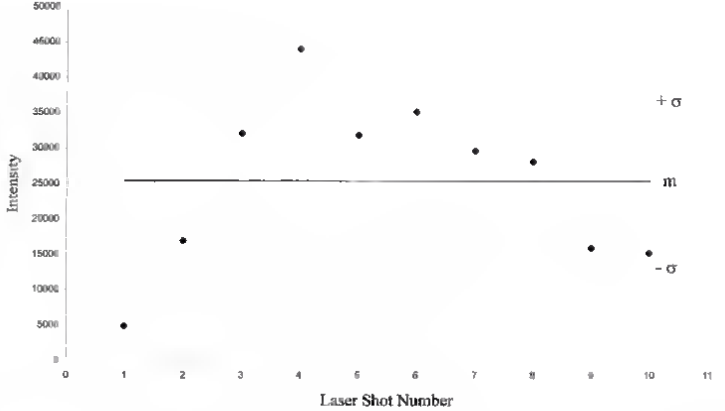
50000
45000
40000
35000
30000
25000
20000
15000
10000
5000
0
Intensity
0
1
2
3
4
5
6
7
8
9
10
11
Laser Shot Number
+ σ
m
- σ

Figure 3-9 Scanning electron micrograph of a porous silicon surface produced by laser modification of a crystalline silicon wafer. The surface is magnified 75 000 times. Image adapted from Anderson *et al.* 2002

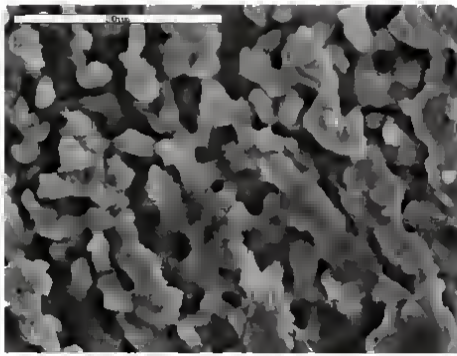

Figure 3-10 Porous silicon etching process. A crystalline silicon wafer was first placed on a piece of silver, which acts as the anode in the etching process. The stack was then placed on a copper flag to allow for electrical contact outside the cell and locked into a Teflon cell, which was sealed with o-rings. A 1:1 etching solution of 48% (w/v) HF and ethanol was added to the Teflon well above the wafer surface. A platinum mesh electrode was submerged in the etching solution so that it sat just above the silicon surface. A constant current density of approximately five microamps was passed through the cell setup from the silver anode to the platinum electrode cathode. In order to expedite the reaction, white light from a tungsten bulb was focused onto the silicon surface during the etching process. The addition of light to this reaction significantly speeds up the process when n-type silicon is used.

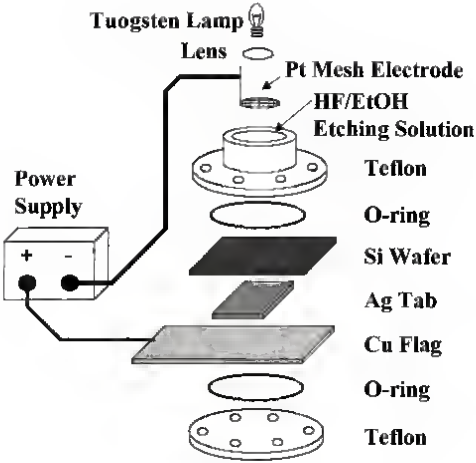
Tuogsten Lamp
Lens
Pt Mesh Electrode
HF/EtOH
Etching Solution
Teflon
Power
Supply
O-ring
+
-
Si Wafer
Ag Tab
Cu Flag
O-ring
Teflon

Figure 3-11 Background mass spectrum of a porous silicon surface. Note that no appreciable chemical background is present in the blank spectrum, unlike the typical background spectrum of MALDI with an organic matrix.

Relative Intensity
100
75
50
25
0
100
150
200
250
300
350
400
450
500
m/z

Figure 3-12 Mixture of acylcarnitines by DIOS-MS The full scan mass spectrum shows the $[M + H]^+$ ions (at m/z 162 m/z 232 and m/z 288 for l-carnitine, isobutylcarnitine and octanoylcarnitine respectively) for each carnitine Note that as with the sample blank spectrum there is a lack of chemical background generated and the there is no fragmentation of the analyte

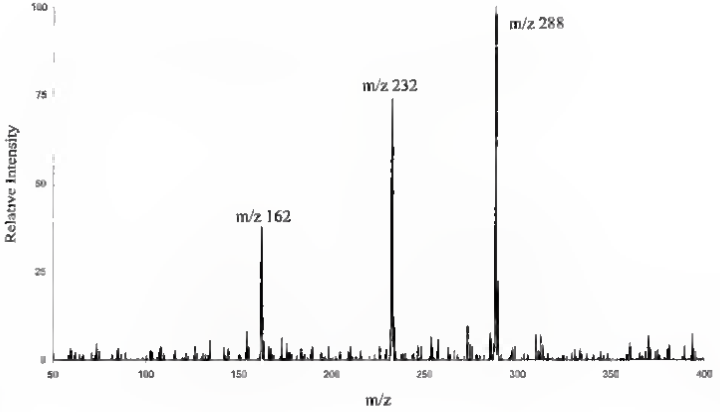
m/z 288
m/z 232
m/z 162
Relative Intensity
m/z
100
75
50
25
0
50
100
150
200
250
300
350
400

Figure 3-13 L-carnitine daughter ions with $[M + H]^+$ ion of isobutyrylcarnitine. The SWIFT isolation window was opened wide enough so that the $[M + H]^+$ ion of the isobutyrylcarnitine internal standard could be isolated along with the $[M + H]^+$ ion of l-carnitine. Once isolated, CID of l-carnitine parent ion at m/z 162 was performed. Note the presence of the charactenstic l-carnitine fragment ion at m/z 103 and the internal standard ion at m/z 232

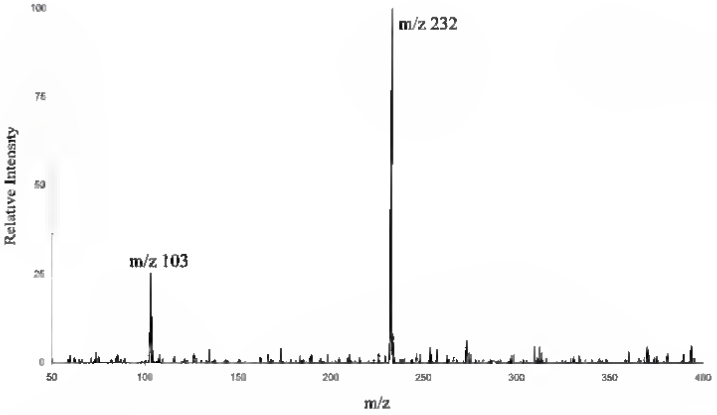
m/z 232
m/z 103
Relative Intensity
m/z
100
75
50
25
0
50
100
150
200
250
300
350
400

Figure 3-14 L-carnitine calibration curve with internal standard by DIOS-MS The calibration plot was constructed by plotting the ratio of ion intensities for m/z 103 and m/z 232 versus the ratio of the masses of the samples deposited on the probe tip Each data point represents the average of three laser spots on the probe tip Each spot is the average of three mass spectra with each mass spectrum made up of five microscans Each microscan consists of three laser pulses Therefore each mass spectrum is the average of fifteen laser pulses and each spot is the average of forty five laser pulses The error bars represent the standard deviation of the mean for each data point

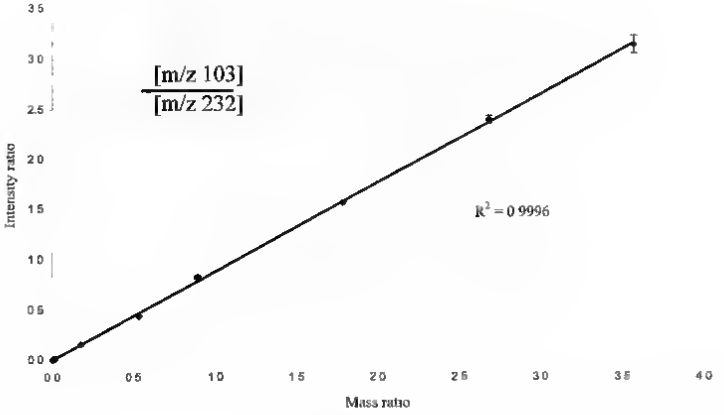
[m/z 103]
[m/z 232]
$R^2 = 0.9996$
Intensity ratio
Mass ratio
0.0
0.5
1.0
1.5
2.0
2.5
3.0
3.5
4.0

Figure 3-15 Octanoylcarnitine daughter ions with $[M + H]^+$ ion of isobutrylcarnitine. The SWIFT isolation window was opened wide enough so that the $[M + H]^+$ ion of the isobutrylcarnitine internal standard could be isolated along with the $[M + H]^+$ ion of octanoylcarnitine. Once isolated, CID of octanoylcarnitine parent ion at m/z 288 was performed. Note the presence of the characteristic octanoylcarnitine fragment ion at m/z 229 and the internal standard ion at m/z 232.

Relative Intensity
100
75
50
25
0
50
100
150
200
250
300
350
m/z
m/z
232
m/z
229

Figure 3-16 Octanoylcarnitine calibration curve with internal standard by DIOS MS The calibration plot was constructed by plotting the ratio of ion intensities for m/z 229 and m/z 232 versus the ratio of the masses of the samples deposited on the probe tip Each data point represents the average of three laser spots on the probe tip Each spot is the average of three mass spectra with each mass spectrum made up of five microscans Each microscan consists of three laser pulses Therefore each mass spectrum is the average of fifteen laser pulses and each spot is the average of forty-five laser pulses The error bars represent the standard deviation of the mean for each data point.

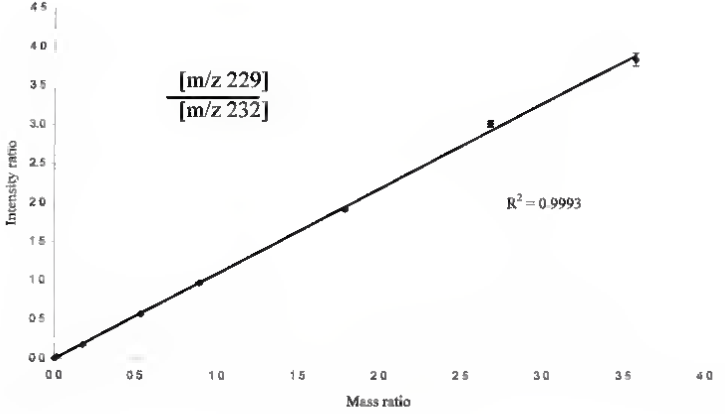
[m/z 229]
[m/z 232]
$R^2 = 0.9993$
Intensity ratio
Mass ratio
0.0
0.5
1.0
1.5
2.0
2.5
3.0
3.5
4.0
4.5
0.0
0.5
1.0
1.5
2.0
2.5
3.0
3.5
4.0

CHAPTER 4
DEVELOPMENT OF AEROGEL MALDI

Background

Recently, a variety of other matrix-free laser desorption techniques have been developed in addition to DIOS. Some of these techniques include desorption of sample off transparent surfaces (Murray *et al.* 2002), crystalline silicon (Bhattacharya & Murray, 2002), silicon thin-film targets (Cuiffi *et al.*, 2001) and organic matrix based sol-gel films (Lin & Chan, 2002). These methods are based on the desire to be able to desorb and ionize biological samples with a laser without producing significant levels of interfering background ions.

Although DIOS-MS has been shown here to be a viable technique for the screening of acylcarnitines, it was desired to find an attractive sample surface capable of generating analyte ions by laser desorption with little or no interfering chemical background that can also be produced consistently from surface to surface. To have more control over the structure of the porous surface than traditional electrochemically etched silicon, aerogel systems were explored as organic matrix-free substrates for laser desorption.

Aerogels are highly porous polymeric compounds that are produced by cross-linking a colloidal dispersion of dissolved monomeric precursors (Kistler, 1932). The resulting rigid gel is supercritically dried to avoid

densification of the pore system. Furthermore, the resultant aerogel is highly porous and easily reproduced. The composition of the aerogel can be precisely controlled and custom surfaces produced by selecting specific monomers or by modification after polymerization. Here, resorcinol-formaldehyde aerogels (LeMay *et al.*, 1990) are characterized as organic-matrix free substrates for laser desorption on a quadrupole ion trap instrument.

Aerogel History

In 1931, Samuel Kistler attempted to form a continuous solid network with similar properties to a wet gel. However, upon drying, the network would shrink, causing cracking of the solid. The shrinking of the structure is caused by the partial crumbling of the pore system due to capillary tension caused by the liquid-vapor interfaces formed during traditional evaporation of solvent. In order to overcome this, supercritical drying of the solvent was employed. This allowed for the transformation of the liquid into a gas without both phases being present in the structure at the same time. This decreases the surface tension that collapses the pores. The resulting highly porous networks were named aerogels (Kistler 1931).

Kistler's original aerogels were created by the aqueous condensation of sodium silicate, forming silica-based aerogels. However, due to advances in the sol-gel process, aerogels can now be formed from a wide assortment of monomers. Organic (Pekala *et al.*, 1992) and inorganic aerogels (Sun & Mark 1969) are now routinely produced. In addition, carbonized aerogels (Kong, 1991) can be formed by partial pyrolysis of organic aerogels in a furnace.

Historically, aerogels have been used for a number of applications. Some of these applications have included wastewater treatment (Ahmed & Atta, 1995), aerocapacitors (Pekala *et al.*, 1994), particle detectors (Henning, 1986) and acoustical insulation (Zimmerman *et al.*, 1995). Furthermore, it has been shown that aerogels can be used as architectural insulators in the form of windows (Herrmann *et al.*, 1995). In this application, one sheet of aerogel exhibits the same insulation value as thirty-two sheets of ordinary glass of comparative thickness. Unfortunately, aerogel cannot yet be produced as fully transparent making this application still to be realized in the future. One of the most popularized applications for aerogel comes from its recent use as a cosmic dust collector aboard the STARDUST project (Tsou, 1995).

Finally, in 2002, an aerogel was produced by scientists at NASA's Jet Propulsion Laboratory that was recognized by Guinness World Records as the world's lightest solid. The silica aerogel weighs only three milligrams per cubic centimeter and is 99.8 % air. In fact, it is quite possibly the lightest solid possible, since the density of air itself is 1.2 mg per cubic centimeter.

Resorcinol-Formaldehyde Aerogel

Currently, aerogels are formed by a sol-gel process that can be broken down into two major steps. First, a sol is formed inside a reaction cell following a series of hydrolysis and condensation reactions. As the gel grows, a three-dimensional network is formed that spans the volume of the reaction cell. At this point, called the gel point, the sol becomes a wet gel, which is a rigid substance that takes the form of the reaction cell. A wet gel consists of a solid part, the rigid

body and a liquid part, which consists of the original solvent of the sol and other byproducts from the condensation reactions, such as water and unreacted monomer.

The second step in the formation of aerogels has to do with the way the wet gel is dried. If the gel is allowed to dry under normal laboratory conditions, the resulting gel, known as a xerogel, will shrink and crack due to capillary forces described earlier. However, if the wet gel is supercritically dried, the system will retain its form and porosity. Wet gels dried in this manner are called aerogels.

For this study, organic aerogels were produced at the Lawrence Livermore National Laboratory from the reaction of resorcinol (1,3 dihydroxybenzene) and formaldehyde, by the reaction shown in Figure 4-1 (Varaganat 1981). Resorcinol adds formaldehyde in the 2, 4, and/or 6 ring positions in polymeric clusters that cross-link to form a wet gel. The 2 position of resorcinol has the highest electron density, but is sterically hindered by the neighboring hydroxyl groups. Therefore, the majority of the reactions occur at the 4 and 6 position of resorcinol.

Under basic conditions, resorcinol reacts with formaldehyde to form a cross-linked wet gel by three principal reactions. First, hydroxymethyl derivatives of resorcinol are formed. Second, the hydroxymethyl derivatives are condensed to form methylene and other methylene ether bridged compounds. Finally, the methylene ether bridges are added to formaldehyde in the manner described above (Wenstler, 1986).

For the production of the aerogels used in this study, resorcinol and formaldehyde were mixed in deionized water at a 1:2 molar ratio. To achieve

pore sizes of approximately 0.1 μm, sodium carbonate was added as a base catalyst (resorcinol/catalyst ratio = 200). This solution was transferred to a glass vial and incubated at 90 °C for seven days. After incubation, the gel was placed in a dilute acid solution for three days to promote cross-linking.

For supercritical drying, the wet gel was placed in acetone in a jacketed pressure vessel and rinsed with acetone a number of times to remove any residual water. After the water had been removed, the acetone was exchanged with liquid carbon dioxide and the gel was dried above the critical point for CO_2 (T_c = 31 °C, P_c = 1100 psi). It is important to exchange the acetone with CO_2 because the critical temperature and pressure for acetone are significantly higher than those for CO_2. This results in a safer drying step due to the lower temperature and pressure necessary to pass the critical point.

Once dried, the remaining bulk RF aerogel, shown in Figure 4-2, is transparent and dark red in color (LeMay et al., 1990). The surface of the aerogel surface, magnified 75,000 times by SEM, is shown in Figure 4-3. The density of the aerogel produced by this set of conditions was 500 mg/cc. When less catalyst is used in the reaction, resulting in a higher resorcinol/catalyst ratio, aerogels of lower density are produced (Pekala & Stone, 1988). Aerogels were produced at densities of 250 mg/cc and 80 mg/cc but these surfaces were difficult to handle, due to their soft structure, and were therefore not used in this study.

Preparation of Aerogel Surfaces for LDMS

For LDMS analysis bulk sections of 500 mg/cc resorcinol-formaldehyde aerogel were sliced into disks (~1mm thick) with a very fine bladed jeweler s saw From these disks 4 mm diameter circular sample surfaces were cut with a cork borer These surfaces were then adhered to the aluminum probe tip with double-sided tape

When the aerogel surface was pipetted with 1 µL of a 10 ppm methanolic solution of spiperone an anti psychotic drug partial collapsing of the pore system is evident upon drying This shrinkage of the surface shown in Figure 4-4 is attributed to compressive stress due to capillary forces on the walls of the pore similar to those avoided during production of the surface by supercritical drying RF aerogels of 250 and 80 mg/cc densities were tested similarly and suffered nearly complete pore collapse These less dense aerogel surfaces are therefore unusable after re-wetting and unfit for this study

To reduce the adverse effects of re-wetting during sample deposition an apparatus was used to electrospray sample onto the aerogel probe tip For this an Analytica electrospray probe high voltage power supply and gas distribution box were assembled (Troendle 2001) Sample was injected by a syringe pump and fed to the electrospray needle through a fused silica capillary The aluminum probe tip with the aerogel surface attached sat on a rotating drum under the electrospray needle in order to apply an even sample layer across the aerogel surface The height of the drum was adjusted so that the width of the spray matched the width of the probe tip This setup is shown in Figure 4-5 Spiperone

samples in methanol were sprayed at 5 μL/min with a sheath gas (nitrogen) flow of 50 mL/min and a electrospray voltage of +4 kV. To insure that no large drops were deposited onto the aerogel surface when the electrospray was first turned on, the spray was started without the aerogel probe tip in place. Once a stable spray was generated, the probe tip was inserted into the apparatus with a plastic rod and the rotating drum was started.

When 1 μL of spiperone was electrosprayed onto the 500 mg/cc aerogel surface, significantly less pore shrinkage is evident than when an equal volume was pipetted onto the surface. This is due to the small solvent droplet size delivered by electrospray and therefore faster solvent evaporation. Although the 250 and 80 mg/cc density aerogels also fared better with electrospray deposition of sample than with traditional pipetting, they both still exhibited too much pore collapse to be used in this analysis. For remainder of analyses discussed here, the 500 mg/cc density resorcinol-formaldehyde aerogel was used. Samples were electrosprayed for 12 s using the apparatus described above in order to achieve a sample volume of approximately 1 μL.

LDMS off Resorcinol-Formaldehyde Aerogel

A mass spectrum generated from a blank RF aerogel surface is shown in Figure 4-6. There is no evidence of residual monomer ions or any other background ions from the aerogel surface. The absence of matrix ions at low m/z values is critical in the detection of small drug molecules and is comparable to the background seen from a porous silicon substrate over the range of low m/z where organic MALDI matrices produce intense background ions.

Figure 4-7 shows a full scan mass spectrum of spiperone from an aerogel surface. At full laser energy, complete fragmentation of spiperone is evident upon ionization off the aerogel surface. This is shown in the production of characteristic fragment ions for spiperone with no detection of the $[M + H]^+$ ion (m/z 396). Proposed fragmentation pathways for each ion are shown in the upper right hand corner of the spectrum.

With the intention of decreasing the laser energy focused onto the sample surface to reduce the extent of fragmentation, the mass spectrometer was modified so that an iris could be placed in the path of the laser source. When the laser energy was attenuated by partially closing the iris, the fragment ion relative intensities decreased and the relative intensity for the $[M+H]^+$ ion increased with the $[M+H]^+$ ion eventually becoming the base peak in the spectrum. This is shown in a plot (Figure 4-8) of ion intensity for each spiperone fragment ion versus iris setting. When MALDI and DIOS spectra were generated at full laser energy (iris fully open) with this setup, no fragmentation of the $[M+H]^+$ ion for spiperone is seen. From this observation, it is clear that the laser energy required to induce fragmentation of spiperone is lower for aerogel MALDI than is seen in the traditional MALDI and DIOS techniques.

In order to determine the amount of laser energy that is focused onto the sample surface, a Molectron (Model #J3-09) laser energy detector was used. The energy detector was first placed in the path of the laser with the iris fully open to allow detection of the entire laser beam. When the laser was fired, the energy detector sent a voltage signal to an oscilloscope. From this signal, the

laser energy per laser pulse could be determined by dividing by a constant inherent to the detector. This process was repeated at multiple settings of the iris. Figure 4-9 is a plot of laser energy per pulse versus the iris setting.

At the iris setting of 100% open, the full laser beam is passed through to the detector. This energy, approximately 370 μJ per pulse, is the energy at which all previous MALDI and DIOS experiments were performed in addition to experiment which produced the spiperone spectrum shown in Figure 4-7. As the iris is closed, the edges of the laser beam are blocked and the remaining beam energy is reduced. The full laser beam is square in shape (as seen unfocused on a sheet of paper) and therefore the first decrease in iris opening resulted in very little reduction in laser energy. However, as the iris blocked more of the laser beam, the laser energy was rapidly attenuated. This is because the spatial intensity distribution of the laser beam is Gaussian in shape.

At an iris setting of 25% open, corresponding to a laser energy of approximately 50 μJ per pulse, spiperone fragment ions are not formed and only the $[M + H]^+$ ion is present. This spectrum is shown in Figure 4-10. The ion intensity for the spiperone ion is comparable to those seen in MALDI and DIOS analyses on the same instrument when analyzed at full laser energies.

To confirm that the ionization process has its basis in the aerogel system acting in place of the MALDI matrix and is not simply traditional matrix-free laser desorption, spiperone was deposited onto the bare aluminum probe tip without organic matrix. Upon analysis in the mass spectrometer, laser desorption of spiperone resulted in the production of no characteristic spiperone ions at any iris

setting. In fact the mass spectrum was identical to the mass spectrum of the bare probe tip blank. It is apparent that the aerogel surface acts in a manner similar to that of the porous silicon surface in DIOS-MS.

The resulting MS/MS spectrum of the $[M + H]^+$ ion of spiperone (m/z 396) obtained by isolation by SWIFT waveform and CID is consistent with ones acquired by MALDI and DIOS methods. This daughter spectrum is shown in Figure 4-11. As with the earlier comparisons with the other desorption ionization techniques, the ion intensities are similar to those generated by MALDI-MS and DIOS-MS.

Signal for the $[M + H]^+$ ion was detectable in full scan mode for spiperone samples as dilute as five parts per billion. This corresponds to approximately 5 pg of spiperone deposited onto the aerogel surface. However, this signal was unsteady and was buried in the baseline signal for most scans. When approximately 10 pg of spiperone were electrosprayed onto the aerogel surface, however, the protonated molecular ion was detected with a signal-to-noise ratio (S/N) of approximately three, as shown in Figure 4-12. For this instrument and aerogel system, this is determined to be the limit of detection. This too is consistent with MALDI detection limits on this particular mass spectrometer.

It should be noted that the amount of sample deposited on the probe tip is the form in which analyte concentration is reported throughout this dissertation. However, only a small fraction of this sample is actually detected during analysis. For example, the aerogel surface used in these analyses is approximately 4 mm in diameter, corresponding to an area of 1.3×10^7 μm^2. The laser beam is

focused to a diameter of 100 μm corresponding to an area of approximately 8 x 10^3 μm^2 From these dimensions less than 0 1% of the sample deposited onto the surface is detected during analysis assuming that the sample has been electrosprayed uniformly across the surface of the aerogel On that basis the mass spectrum in Figure 4-12 corresponds to the desorption of 10 fg of spiperone Of course this calculation neglects the depth of the sample layer and the amount that the laser penetrates into this layer Thus, a reasonable estimate for the limit of detection for spiperone in a standard for aerogel MALDI is 10 pg deposited on the aerogel surface 10 fg in a single laser spot

Conclusion

It has been shown here that resorcinol-formaldehyde aerogel substrates are potentially valuable for laser desorption mass spectrometry Chemical background at low mass-to-charge resulting from the surface is significantly reduced versus traditional MALDI matrix background This allows for simple analysis of low molecular weight compounds such as small drug molecules

The production of aerogel surfaces should be more reproducible than electrochemically etched porous silicon surfaces due to the use of the sol-gel process and more importantly the supercritical drying of the surface to avoid pore collapse Furthermore the production of porous silicon surfaces cannot be generated with as much precision because the electrochemical etching process is susceptible to imperfections in the crystalline silicon wafer (Canham 1997) Also although only resorcinol-formaldehyde aerogels are discussed here, aerogels can be produced from a variety of monomers, some of which could

exhibit qualities amenable to laser desorption comparable or better than those described here

Ion intensities generated for spiperone using RF aerogel substrates are comparable to traditional MALDI and DIOS However, the addition of an organic matrix is not necessary in the aerogel MALDI technique Furthermore, RF aerogels were stable at room temperature for long periods of time after production without further reaction unlike porous silicon The aerogel surfaces used in this study were taken from a bulk section of aerogel that was stored in the dark at room temperature over the course of one year without visual degradation of the surface However, the electrochemically etched porous silicon used in this study would corrode over the course of one week after production

Optimum laser energy for the ionization of spiperone is significantly lower for RF aerogel substrates than for MALDI and DIOS This is shown by the complete fragmentation of spiperone when full laser power is focused on the sample However, with reduced laser energies aerogel MALDI signals are quite similar to traditional MALDI and DIOS spectra

Figure 4-1 Reaction of resorcinol and formaldehyde to produce RF-aerogel. Under basic conditions, resorcinol reacts with formaldehyde to form a cross-linked wet gel by three principal reactions. First, hydroxymethyl derivatives of resorcinol are formed. Second, the hydroxymethyl derivatives are condensed to form methylene- and other methylene ether-bridged compounds. Finally, the methylene ether bridges are added to formaldehyde at the 2, 4 and 6 positions.

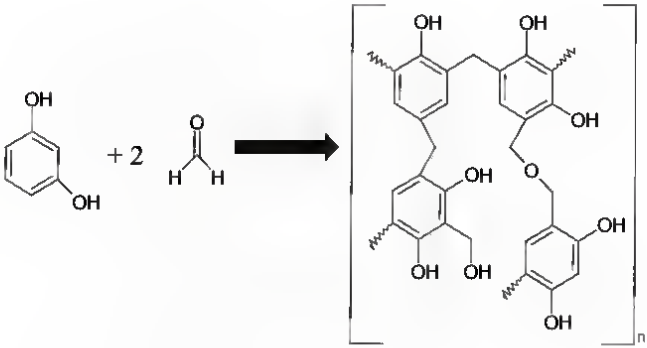
OH
OH
+ 2
O
H
H
OH
OH
OH
OH
O
OH
OH
OH
OH
n

Figure 4-2 Aerogel bulk photo. Once supercritically dried, bulk RF aerogel is transparent and dark red in color

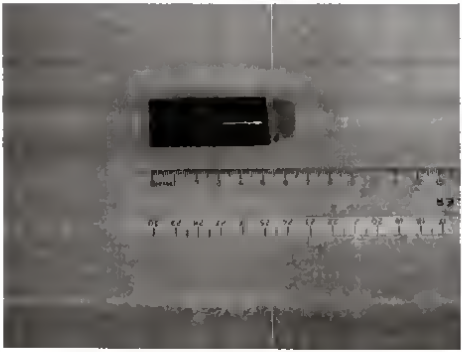

Figure 4-3 Scanning electron micrograph of aerogel surface The surface of the aerogel surface is magnified 75 000 times by SEM

Figure 4-4 Photomicrograph (magnification = 40x) of a piece of RF aerogel before and after wetting. When the aerogel surface (500 mg/cc) was spotted with 1 μL of a 10 ppm methanolic solution of spiperone, partial collapsing of the pore system is evident upon drying. This shrinkage of the surface is attributed to compressive stress due to capillary forces on the walls of the pore similar to those avoided during production of the surface by supercritical drying. A larger piece of aerogel is used in this experiment than is used for LDMS analysis to better show the collapse of the surface.

$\rho = 500$ mg/cm^3

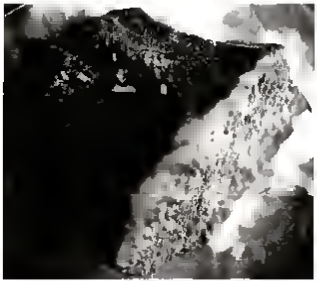

Before

After

Figure 4-5 Electrospray apparatus An apparatus was constructed to electrospray sample onto the aerogel probe tip in order to reduce the adverse effects of re-wetting during sample deposition Sample solution was injected by a syringe pump and fed to the electrospray needle through a fused silica capillary The probe tip sat on a rotating drum under the electrospray needle in order to apply an even sample layer across the aerogel surface The height of the drum was adjusted so that the width of the spray matched the width of the probe tip

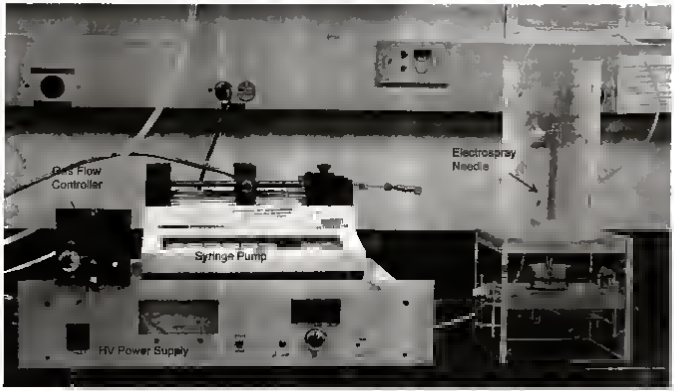
Gas Flow
Controller
Electrospray
Needle
Syringe Pump
HV Power Supply

Figure 4-6 RF aerogel background mass spectrum at full laser power. There is no evidence of residual monomer ions or any other background ions from the aerogel surface. The absence of matrix ions at low m/z values is critical in the detection of small drug molecules and is qualitatively comparable to the background seen from a porous silicon substrate over the range of low m/z where organic MALDI matrices often produce background ions. This spectrum was generated from one analytical scan comprised of three microscans. Each microscan consists of three laser pulses. Therefore, the spectrum is the average of nine laser pulses. The absolute intensity of the spectrum is set relative to 45 000 counts = 100%. This is directly comparable to the relative intensity scale for the aerogel MALDI spectrum of spiperone in Figure 4-10.

Relative Intensity
100
75
50
25
0
50
100
150
200
250
300
350
400
450
500
550
600
m/z

Figure 4-7 Mass spectrum of spiperone by aerogel MALDI at full laser power. At full laser energy, complete fragmentation of spiperone is evident upon ionization off the aerogel surface. This is shown in the production of characteristic fragment ions for spiperone with no detection of the $[M + H]^+$ ion (m/z 396). Assignments for each fragment ion are shown in the upper right hand corner of the spectrum. This spectrum was generated from one analytical scan comprised of three microscans. Each microscan consists of three laser pulses. Therefore, the spectrum is the average of nine laser pulses.

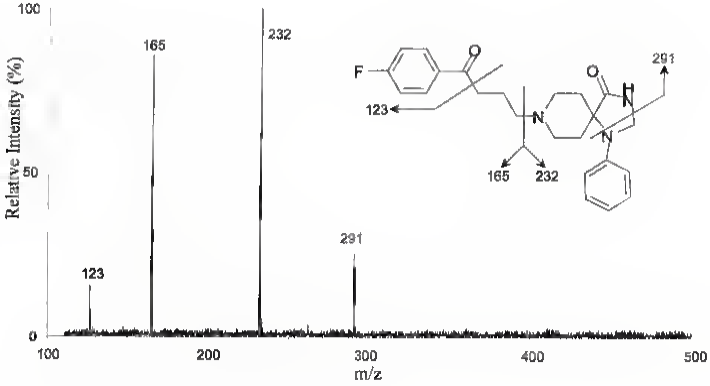
100
50
0
Relative Intensity (%)
165
232
291
123
100
200
300
400
500
m/z
F
O
O
N
H
N
123
165
232
291

Figure 4-8 Fragmentation of spiperone versus laser power. When the laser energy was attenuated by partially closing the iris, the fragment ion relative intensities decreased and the $[M+H]^+$ ion became the base peak in the spectrum. In this graph, the relative ion intensity for each spiperone fragment ion is plotted versus the iris setting.

Relative Intensity
100
75
50
25
0
0
25
50
75
100
Iris Setting (% open)
(M + H)+, m/z 396
m/z 165
m/z 291
m/z 123
m/z 232

Figure 4-9 Laser power versus iris setting. A Molectron laser energy detector was first placed in the path of the laser with the iris fully open to allow detection of the entire laser beam. When the laser was fired, the energy detector sent a voltage signal to an oscilloscope. From this signal, the laser energy per laser pulse could be determined by dividing by a constant inherent to the detector. This process was repeated at multiple positions of the iris. When the iris is in the 0% open setting, there is still an opening of approximately 1 mm for the laser beam to pass through. This accounts for the non-zero laser power reading at the iris setting of 0 % open.

Laser Energy (μJ/pulse)
400
350
300
250
200
150
100
50
0
0
25
50
75
100
Iris Setting (% open)

Figure 4-10 Spiperone mass spectrum by aerogel MALDI at an iris setting of 25% open. This corresponds to a laser energy of approximately 50 μJ per pulse. This spectrum was generated from three microscans. Each microscan consists of three laser pulses. Therefore, the spectrum is the average of nine laser pulses.

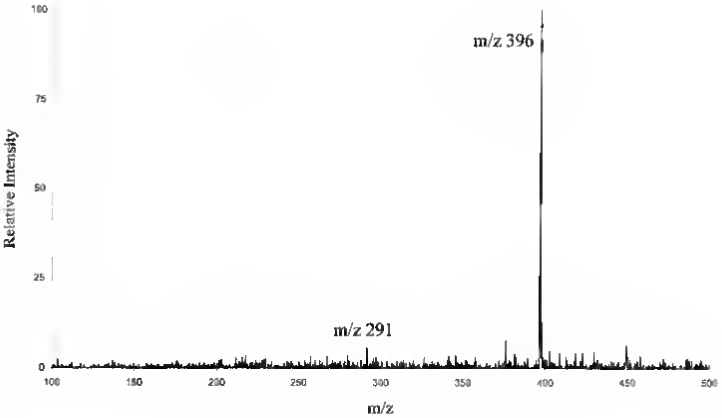
m/z 396
m/z 291
Relative Intensity
m/z
100
75
50
25
0
100
150
200
250
300
350
400
450
500

Figure 4-11 Spiperone daughter spectrum by aerogel MALDI Upon isolation by SWIFT waveform and CID of the $[M + H]^+$ ion of spiperone (m/z 396) the resulting MS/MS spectrum is consistent with ones acquired by MALDI and DIOS methods

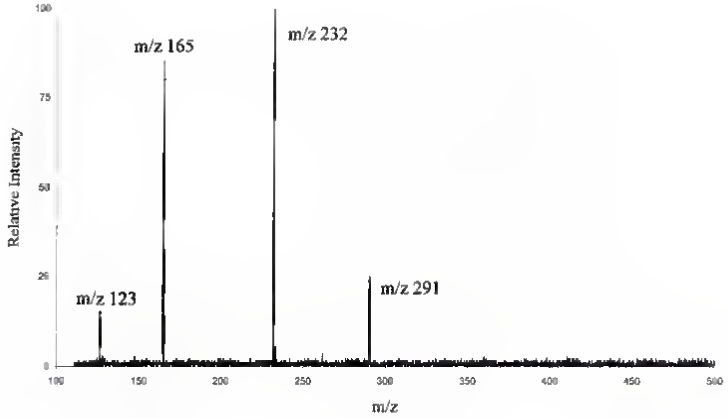
m/z 165
m/z 232
m/z 123
m/z 291
Relative Intensity
m/z
100
75
50
25
0
100
150
200
250
300
350
400
450
500

Figure 4-12 Spiperone detection limit by aerogel MALDI. When approximately 10 picograms of spiperone were electrosprayed onto the aerogel surface, the protonated molecular ion was detected with a signal to noise ratio (S/N) of approximately three at an ion setting of 25% open. The spectrum is the average of nine laser pulses. For this instrument and aerogel system, this is determined to be the limit of detection.

m/z 396
Relative Intensity
m/z
100
75
50
25
0
50
100
150
200
250
300
350
400
450
500

CHAPTER 5
CARNITINE ANALYSIS BY AEROGEL MALDI

Csmitine Analysis

For the analysis of acylcarnitines by aerogel MALDI, a mixture of l-carnitine isobutrylcarnitine and octanoylcarnitine was electrosprayed onto a 500 mg/cc aerogel surface The spray time was monitored so that approximately ten nanograms of each analyte were deposited on the probe tip The full scan mass spectrum at an iris setting of 25% open is shown in Figure 5-1 As seen previously in the spectra for spiperone the spectrum is primarily protonated molecular ions for each of the acylcarnitines at the reduced laser power In this case the peaks at m/z 162 m/z 232 and m/z 288 represent the $[M + H]^+$ ions for l-carnitine isobutrylcarnitine and octanoylcarnitine, respectively

Based on the preliminary aerogel MALDI experiments with spiperone it was hypothesized that the daughter ions produced from MS analysis of acylcarnitines using aerogel surfaces would be similar in fragmentation pattern and relative intensities versus those seen with traditional MALDI and DIOS To confirm this for acylcarnitines daughter spectra for l-carnitine and octanoylcarnitine were generated in order to determine the characteristic MS/MS ions for each compound These spectra are shown in Figure 5-2 for l-carnitine and Figure 5-3 for octanoylcarnitine

For l-carnitine the parent ion at m/z 162 was isolated and fragmented by CID at an amplitude of 800 mV. This resulted in the production of significant daughter ions at m/z 103, corresponding to the neutral loss of 59 amu, and m/z 60, which results from the protonation of the trimethylamino functionality. There is also a small peak at m/z 85 that corresponds to the losses of the trimethylamino group and the fatty acid functionality.

Although the ion at m/z 60 produces the most abundant signal in this MS/MS spectrum for l-carnitine, it cannot be used as the quantitation ion in this analysis for two reasons. First, the ion at m/z 60 is a charactenstic ion for all acylcarnitines and it cannot be guaranteed that all signal at that m/z value has been generated by the analyte of interest. The presence of an interfering ion at m/z 60 is usually unlikely, due to the isolation of the parent ion in a tight isolation window. However, in this analysis, the isolation window is opened wide so that the isobutrylcarnitine internal standard ion can be seen as well. This may allow for the production of fragment ions from other acylcarnitines to be present in the daughter spectrum.

The second reason the daughter ion at m/z 60 cannot be used in this analysis is based on the low mass cut-off (LMCO) that is inherent to the Ion trap instrument. When an ion is selected for MS/MS analysis, it is first isolated at a specific q value. After isolation, the parent ion is moved to a lower q value. This is so that any daughter ions produced upon CID of the parent ion will remain stable in the trap (recall that Ions line up from left to right along the $a_z = 0$ line from high m/z values to low m/z values).

However since both l-carnitine and octanoylcarnitine are isolated and fragmented at the same set of q values the LMCO will be different for each compound This can be shown by the equation $m_1q_1 = m_2q_2$ which was introduced in Chapter Two For l-carnitine m_1 is 162 and q_1 is 0 2 corresponding to the $[M + H]^+$ ion for l carnitine and the q value of isolation The variable m_2 is the LMCO value and q_2 is 0 908 corresponding to the q value of ejection When the equation is solved for m_2 an LMCO value is shown to be 36 amu This means that any daughter ions of l-carnitine with an m/z value lower than 36 amu will not be stable in the ion trap and will be ejected before the analytical scan step

For octanoylcarnitine since the q values for excitation and ejection are the same as those used in the l-carnitine experiment the calculation is the same except for the substitution of m/z 288 for m_1 Upon solving the equation for m_2 for octanoylcarnitine the LMCO value is established to be 63 amu This means that no ion with an m/z value less than 63 amu will be stable in the ion trap This includes the characteristic acylcarnitine ion at m/z 60 It is for this reason that the daughter ion at m/z 103 in the l-carnitine MS/MS spectrum was used for quantitation

The MS/MS spectrum for octanoylcarnitine shows typical daughter ions at m/z 229, m/z 127 and m/z 85 The ion at m/z 229 corresponds to the loss of the trimethylamino functionality and is the base peak This ion was used for quantitation experiments Less intense daughter ion are evident in the spectrum at m/z 127 and m/z 85 The ion at m/z 127 corresponds to the loss of the

carnitine backbone and is characteristic of all acylcarnitines. The ion at m/z 85 has been described earlier and is another characteristic acylcarnitine daughter ion. Note that the characteristic daughter ion at m/z 60 is not present in the spectrum. This is because of the LMCO issues described above. In fact, upon close inspection, it is shown that signal is not generated at m/z values less than 63 amu in this spectrum.

Blood Spot Sample Extraction

The previous calibration curves discussed in this dissertation have been made by analyzing acylcarnitine samples as pure standard solutions in methanol. However, since it is desired to determine the concentration level of acylcarnitines from a whole blood sample, calibration of the analyte within an extracted biological matrix would give a much better representation of the quantitative ability of the technique for biomarker screening. For this reason, the calibration curves for l-carnitine and octanoylcarnitine generated by the aerogel MALDI technique were constructed by extracting whole blood into a methanolic solution spiked with acylcarnitine standards.

As mentioned in Chapter 1, a blood sample is taken from all newborns in the state of Florida within the first two days after birth. This is done by pricking the heel of the child with a small needle and collecting blood on a filter paper index card, known as a Guthrie Card (Guthrie & Susi, 1963). For analysis here, all blood samples were taken from and by the author to alleviate any concerns for safety.

Blood samples were taken by lancing the pad of the thumb, which had previously been cleaned with soap and water, dried and swabbed with methanol. The thumb was applied to a Guthrie Card, acquired from the Birth Center of Gainesville, and blood was collected until each of the five sample spots were saturated. The card was allowed to dry over a period of one hour, at which time the card was stored in a desiccator for further use.

For analysis of the blood sample, a circular piece of the filter paper card containing blood was cut out using a hole punch. This filter paper sample was then placed in an Eppendorf tube with one milliliter of methanol and vortexed for five minutes. After vortexing, the filter paper was removed from the Eppendorf tube and discarded. The remaining methanolic sample was then used as the extracted whole blood sample.

Blood Spot Analysis

For MS analysis of the whole blood extract, approximately one microliter of the methanolic sample was electrosprayed onto an aerogel surface. As with the electrosprayed spiperone samples, minimal pore collapse of the aerogel surface was observed. The resulting full scan mass spectrum is shown in Figure 5-4 and contains a high chemical background with peaks at every m/z value. This is because whole blood is made up of a variety of proteins and many other compounds. However, this was not a problem in this analysis because the use of MS/MS provides the selectivity necessary for the detection of the compounds of interest. This is due to the fact that the isolation and CID steps take place at discrete ion frequencies and therefore only affect the selected ions of interest.

In order to construct calibration curves for l-carnitine and octanoylcarnitine it was first necessary to create a set of extractions separate to those used in the background analysis. For these calibration extractions standard samples of l-carnitine, octanoylcarnitine and the internal standard isobutyrylcarnitine were spiked onto the filter paper card and allowed to dry before placing the card in the methanol solution. The analyte solutions were added before extraction into methanol in order to limit error due to extraction efficiencies and dilution in the subsequent samples that were analyzed without prior spiking of acylcarnitines. These latter samples include whole blood samples of unknown acylcarnitine concentrations that are to be tested after construction of the calibration curves.

Standard solutions of l-carnitine and octanoylcarnitine, at levels ranging from one hundred nanograms deposited to one hundred picograms deposited for each compound, were spiked onto a series of filter paper spots containing whole blood. A solution of isobutyrylcarnitine was added to each spot, at a level of twenty-five nanograms added. Once the spiked filter paper blood spots were dry they were cut out and extracted into one milliliter of methanol by vortexing for five minutes. After vortexing, the filter paper was removed and the remaining solution was used for analysis by aerogel MALDI. Each solution was electrosprayed onto an aerogel surface and analyzed by MS in accordance with methods described earlier.

Figure 5-5 shows the full scan mass spectrum of an extracted blood spot sample that was previously spiked with an acylcarnitine mixture. In this case

fifty nanograms of l-carnitine and octanoylcarnitine were added to the sample in addition to the twenty-five nanograms of internal standard The protonated molecular ions for each compound at m/z 162 for l-carnitine m/z 232 for isobutrylcarnitine and m/z 288 for octanoylcarnitine are clearly seen above the chemical background of the biological matrix However as the concentration for the standards decreased the sample peaks were once again buried within the background

In order to isolate and fragment the analyte ions the wide SWIFT isolation window described earlier for DIOS analysis was once again used This window allowed both the internal standard ion and the parent ion of either l-carnitine or octanoylcarnitine to be retained in the trap while ions of higher and lower m/z values were removed After isolation the parent ion at either m/z 162 for l-carnitine analysis or m/z 288 for octanoylcarnitine analysis was fragmented by CID The resulted in a MS/MS spectrum in which the daughter ions of the analyte was present along with the protonated molecular ion of the internal standard

Recall that all ions with an m/z value within those of the analyte and the internal standard will also be retained in the trap during isolation This produced a daughter spectrum with a high chemical background within the isolation window and relatively no background at m/z values higher or lower than the window An example of this spectrum is shown in Figure 5-6 Note that the internal standard ion stands above the chemical background at a level of twenty-five nanograms added The notch cut out of the background around a m/z value

of 288 is present because the ions in this region corresponding to $[M + H]^+$ ion of octanoylcarnitine in this case have been fragmented and are responsible for the daughter ions at lower m/z values m/z 229 and m/z 127

A calibration curve was constructed for l-carnitine by plotting the ratio of the l-carnitine daughter ion at m/z 103 and the isobutrylcarnitine $[M + H]^+$ ion at m/z 232 versus the ratio of concentrations of l-carnitine and isobutrylcarnitine on the aerogel surface This plot is shown in Figure 5-7 A similar calibration curve for octanoylcarnitine was constructed using the octanoylcarnitine daughter ion at m/z 229 and the internal standard ion at m/z 232 This plot is shown in Figure 5-8

For each calibration curve each data point represents the average of three sampling spots on the aerogel surface Three mass spectra were collected and averaged at each sampling spot with each mass spectrum made up of five microscans Each microscan consists of three laser pulses Therefore each mass spectrum is the average of fifteen laser pulses and forty-five laser pulses were fired and averaged at each sampling spot The error bars represent the standard deviation of the mean for each data point

Note that the error bars for each point shows that there is good precision for this analysis Furthermore the data points exhibit good correlation with the trend line for each compound The major source of error within this analysis can be traced to the extraction of the analytes into the methanol solution Regardless of this error the curves generated correlated well with three blood samples spiked with known concentrations of l-carnitine and octanoylcarnitine As with

the calibration curves generated by the DIOS method the concentrations of each of the three tests mixtures were extrapolated from the curve within ten percent of their actual values

Unknown Blood Spot Concentration

Finally a blood sample was prepared for analysis without any spiking of l-carnitine or octanoylcarnitine Fresh liquid blood was spotted onto a clean filter paper card and dried A piece of this dried blood spot was punched out and twenty-five nanograms of isobutrylcarnitine were added as an internal standard The blood spot was then extracted into methenol as described earlier and electrosprayed onto an aerogel surface for MS analysis

From extrapolation from the calibration curves it was determined that the concentration of l-carnitine in the blood sample was 10 ppm and the concentration of octanoylcarnitine was 3 ppm This fits well with the typical concentration ranges of 3 ppm to 13 ppm for l carnitine and 1 ppm to 6 ppm for octanoylcarnitine Furthermore, the molar ratio of octanoylcarnitine to l-carnitine is 0 17 (62 μM for l-carnitine and 10 5 μM for octanoylcarnitine) which is also within the normal range. This is to be expected because the author has no history of metabolic disease

Figure 5-1 Mass spectrum of carnitine mixture by aerogel MALDI. The full scan mass spectrum was taken at an iris setting of 25% open. As seen previously in the spectra for spiperone, the spectrum is primarily protonated molecular ions for each of the acylcarnitines. In this case, the peaks at m/z 162, m/z 232 and m/z 288 represent the $[M + H]^+$ ions for l-carnitine, isobutyrylcarnitine and octanoylcarnitine, respectively

m/z 162
m/z 232
m/z 288
Relative Intensity
m/z
100
75
50
25
0
100
150
200
250
300
350
400
450
500
550
600

Figure 5 2 Daughter spectrum of l-carnitine by aerogel MALDI The parent ion for l carnitine at m/z 162 was isolated and fragmented by CID at an amplitude of 800 mV This resulted in the production of significant daughter ions at m/z 103 corresponding to the neutral loss of 59 amu, and m/z 60 which results from the protonation of the trimethylamino functionality There is also a small peak at m/z 85 that corresponds to the losses of the trimethylamino group and the fatty acid functionality

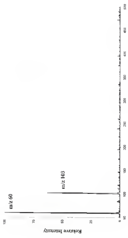

m/z 60
m/z 103
Relative Intensity
m/z
0
25
50
75
100
50
100
150
200
250
300
350
400
450
500

Figure 5-3 Daughter spectrum of octanoylcarnitine by aerogel MALDI. The parent ion for octanoylcarnitine at m/z 288 was isolated and fragmented by CID at an amplitude of 600 mV. This resulted in the production of significant daughter ions at m/z 229, m/z 127 and m/z 85. The ion at m/z 229 corresponds to the loss of the trimethylamino functionality and is the base peak. This ion was used for quantitation experiments. Less intense daughter ion are evident in the spectrum at m/z 127 and m/z 85. The ion at m/z 127 corresponds to the loss of the carnitine backbone and is characteristic of all acylcarnitines. The ion at m/z 85 has been described earlier and is another characteristic acylcarnitine daughter ion.

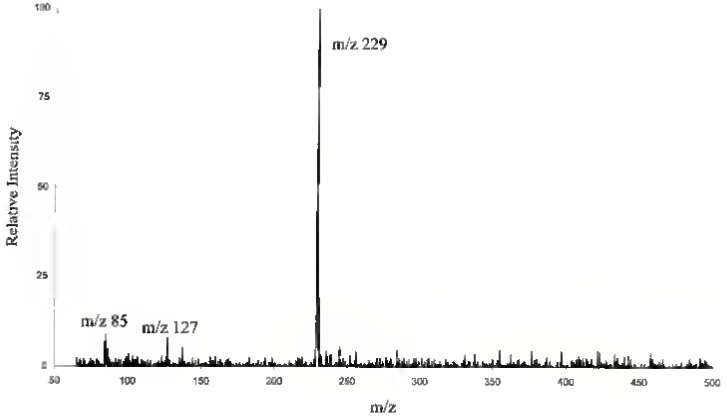
100
75
50
25
0
Relative Intensity
m/z 229
m/z 85
m/z 127
50
100
150
200
250
300
350
400
450
500
m/z

Figure 5-4 Full scan mass spectrum of whole blood extract by aerogel MALDI. The spectrum contains a high chemical background with peaks at every m/z value. This is because whole blood is made up of a variety of proteins and many other compounds.

Relative Intensity
100
75
50
25
0
100
150
200
250
300
350
400
450
500
550
600
m/z

Figure 5-5 Full scan mass spectrum of whole blood extract spiked with acylcarnitine standards by aerogel MALDI. Fifty nanograms of l-carnitine and octanoylcarnitine were added to the sample in addition to the twenty five nanograms of internal standard. The protonated molecular ions for each compound at m/z 162 for l-carnitine, m/z 232 for isobutrylcarnitine and m/z 288 for octanoylcarnitine are clearly seen above the chemical background of the biological matrix

m/z 162
m/z 232
m/z 288
Relative Intensity
m/z
100
75
50
25
0
100
150
200
250
300
350
400
450
500
550
600

Figure 5-6 Daughter spectrum of octanoylcarnitine with internal standard within the wide isolation window. This wide isolation allowed both the internal standard ion and the parent ion of octanoylcarnitine to be retained in the trap while ions of higher and lower m/z values were removed. After isolation, the parent ion at m/z 288 for octanoylcarnitine analysis was fragmented by CID. Note that the internal standard ion stands above the chemical background. The notch cut out of the background around a m/z value of 288 is present because the ions in this region, corresponding to $[M + H]^+$ ion of octanoylcarnitine, have been fragmented and are responsible for the daughter ions at lower m/z values, m/z 229 and m/z 127.

Relative Intensity
100
75
50
25
0
100
150
200
250
300
350
400
m/z
m/z 127
m/z 229
m/z 232
m/z 268

Figure 5-7 Calibration curve for l-carnitine versus an internal standard by aerogel MALDI Each data point represents the average of three sampling spots on the aerogel surface Three mass spectra were collected and averaged at each sampling spot with each mass spectrum made up of five microscans Each microscan consists of three laser pulses Therefore each mass spectrum is the average of fifteen laser pulses and forty-five laser pulses were fired and averaged at each sampling spot The error bars represent the standard deviation of the mean for each data point

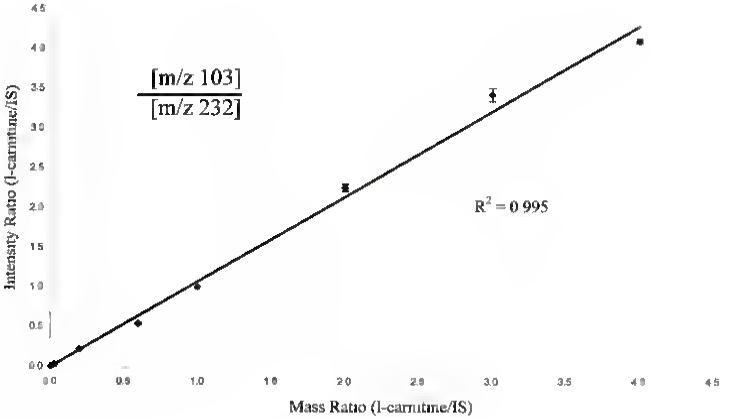
[m/z 103]
[m/z 232]
R² = 0.995
Intensity Ratio (l-carnitine/IS)
Mass Ratio (l-carnitine/IS)
0.0
0.5
1.0
1.5
2.0
2.5
3.0
3.5
4.0
4.5

Figure 5-8 Calibration curve for octanoylcarnitine versus an internal standard by aerogel MALDI. Each data point represents the average of three sampling spots on the aerogel surface. Three mass spectra were collected and averaged at each sampling spot with each mass spectrum made up of five microscans. Each microscan consists of three laser pulses. Therefore, each mass spectrum is the average of fifteen laser pulses and forty-five laser pulses were fired and averaged at each sampling spot. The error bars represent the standard deviation of the mean for each data point.

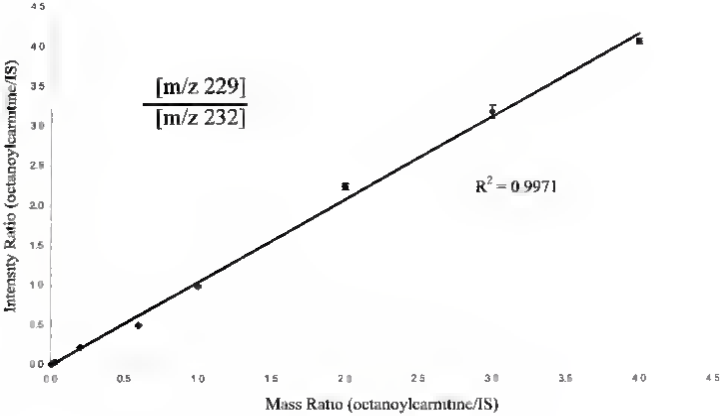
[m/z 229]
[m/z 232]
$R^2 = 0.9971$
Intensity Ratio (octanoylcarnitine/IS)
Mass Ratio (octanoylcarnitine/IS)
0.0
0.5
1.0
1.5
2.0
2.5
3.0
3.5
4.0
4.5

CHAPTER 6
CONCLUSIONS AND FUTURE WORK

Conclusions

Laser desorption ionization techniques such as matrix-assisted laser desorption/ionization mass spectrometry (MALDI-MS) have traditionally employed an organic matrix to enhance ionization efficiency of a sample (Karas & Hillenkamp 1988). The matrix plays a major role in the ionization process by spatially separating the analyte molecules, absorbing laser energy, and donating protons to the ion plume (Zenobi & Knochenmuss 1998). However, a major drawback to MALDI-MS is the intense low mass-to-charge ion background that arises from the organic matrix. Matrix-free techniques have been recently introduced in which the sample surface plays the part of the organic matrix without producing the high chemical background. With desorption/ionization on porous silicon (DIOS), the analyte is spotted on electrochemically etched porous silicon and no additional organic matrix is added (Wei *et al.* 1999). The resulting mass spectra are similar to MALDI spectra but without the organic matrix background. However, the production of porous silicon is not entirely reproducible, which can lead to inconsistent MS data. The development of a new, more rugged, matrix-free laser desorption technique, called aerogel MALDI, was first reported in this dissertation.

Aerogels are highly porous polymeric solids produced by cross-linking a colloidal dispersion of dissolved monomeric precursors (Kistler 1932). The resulting rigid gel is supercritically dried to avoid densification of the pore system and the resultant aerogel is highly porous and easily reproduced. The composition of the aerogel can be precisely controlled and custom surfaces produced by selecting specific monomers or by modification of the surface after polymerization. For this study, resorcinol-formaldehyde (RF) aerogels were characterized as organic-matrix free substrates for laser desorption on a quadrupole ion trap mass spectrometer.

Upon MS analysis of RF aerogel surfaces, a reduced background signal compared to MALDI spectra was observed and no significant ion signal was present from the aerogel's monomers resorcinol (m/z 110) and formaldehyde (m/z 30). To evaluate the aerogel's ability to generate mass spectra of small drug molecules, the anti-psychotic drug spiperone (MW 396) was characterized using RF aerogel (ρ = 500 mg/cc).

When the aerogel surface was spotted with a methanolic sample, some collapsing of the pore system was evident upon drying. This shrinking of the surface is attributed to compressive stress due to capillary forces. To minimize this, sample was electrosprayed onto the aerogel surface, which resulted in decreased pore shrinkage due to smaller solvent droplets and faster solvent evaporation.

At full laser power, the analyte underwent nearly 100% fragmentation. By placing an iris in the path of the laser beam, the laser power was varied and

optimized to reduce fragmentation. At attenuated laser powers, significantly less fragment ions of spiperone were observed. Tandem mass spectra (MS/MS) were generated and were consistent with MALDI-MS/MS data previously produced in both relative ion intensity and fragmentation pattern.

To test the quantitative ability of the aerogel MALDI technique in the analysis of small biomolecules, the biomarkers attributed to the metabolic disorder medium-chain acyl-CoA dehydrogenase deficiency (MCADD), l-carnitine and octanoylcarnitine, were analyzed. In order to screen for MCADD, the relative concentration of both biomarkers must be determined from whole blood samples. For this, calibration curves were generated using an internal standard for each compound and compared to curves produced by MALDI-MS and DIOS-MS analyses.

It was shown here that resorcinol-formaldehyde aerogel substrates are valuable for laser desorption mass spectrometric analysis of low molecular weight compounds, such as acylcarnitines. Relative ion intensities generated by aerogel MALDI are comparable to traditional MALDI and DIOS. However, the reduced chemical background attributed to aerogel MALDI allows for the analysis of biomolecules that would normally be interfered with by organic MALDI matrices. Furthermore, RF aerogels are precisely constructed at the nanometer scale, allowing for more consistent production and analysis over porous silicon because the super-critically dried aerogel pore system does not collapse during drying (Amato *et al.* 1997).

The concept of using a laser-based ionization method coupled to a mass spectrometer was introduced earlier for screening biomarkers in the detection of metebolic disorders (Belford & Yost, 2001). The use of laser desorption ionization mass spectrometry for screening is beneficial because laser based techniques like MALDI, DIOS and aerogel MALDI require little sample preparation and can often tolerate relatively dirty biological samples. For example, in this study, whole blood extracts were analyzed by aerogel MALDI without any clean-up steps besides the methanolic extraction. Furthermore, laser-based methods do not require the time that a chromatographic separation does for analysis. These two characteristics of laser-based ionization methods are beneficial to the screening process.

One drawback of laser based ionization methods is their limited quantitative capabilities. However, it was shown here that these techniques can generate sufficient precision with the use of internal standards for screening. This is true because the goal of the screening process is to determine when biomarkers are present in a sufficient enough concentration to require a more in-depth analysis. It is not the goal of the screening method to be the final diagnostic test. Any samples responding positively to the screening process could be examined more closely by other techniques, while samples responding negatively could be reported as normal.

The desorption-ionization process for DIOS was described in Chapter 3. In short, the porous silicon surface acts in a manner similar to the organic matrix in MALDI. In this process, the matrix plays a series of roles (Shen *et al.*, 2001)

First the excess in which the organic matrix is added (generally 1000-to-1) to the probe tip allows for analyte molecules to be separated spatially from one another This insures that the matrix and not the analyte absorbs the majority of the laser energy Second, matrix absorbs the ultraviolet radiation from the laser and transfers it to the analyte This allows for one matrix to ionize a series of compounds as opposed to traditional laser desorption where the wavelength of the laser must be changed to match the wavelength at which each compound will absorb Finally, the matrix is involved in the gas-phase proton transfer to the analyte This is evident in the typical presence of $[M + H]^+$ ions in MALDI and the acidic nature of most organic matrices

In DIOS the analyte is trapped within the structure of the porous silicon along with solvent When the laser is focused onto the porous silicon surface the radiation is absorbed by the surface and transferred to the analyte It is believed that the desorption of solvent, in addition to analyte aids in providing the protons necessary to produce $[M + H]^+$ analyte ions in DIOS (Kruse *et al.* 2001)

For aerogel MALDI it is proposed in this dissertation that the desorption-ionization process closely follows this model This is based on close similarities between the two techniques and the resulting mass spectra Although the liquid sample is electrosprayed allowed to dry before analysis by aerogel MALDI, it is expected that some solvent is retained within the pore structure of the aerogel surface When radiation from the nitrogen laser is focused onto this surface it is believed that both analyte and solvent are desorbed into the gas phase where

the analyte can accept proton and produce $[M + H]^+$ ions. Since there is no addition of organic matrix and the polymeric structure can withstand the energy of the focused laser, there are no other ionization events aside from sample impurities and environmental contaminants and the aerogel surface. This results in a mass spectrum that is primarily comprised of analyte signal with a limited chemical background. Furthermore, since $[M + H]^+$ ions are produced for the analyte at laser powers less than those necessary for MALDI and DIOS, it is proposed that the transfer of laser energy to the aerogel surface and then to the analyte is more efficient than the transfer of laser power to the porous silicon and then to the analyte in DIOS.

Future Work

Although the biomarkers for the metabolic disorder MCADD, l-carnitine and octanoylcarnitine, were focused on in this study, a multitude of biomarkers for a number of disorders could be tested for within a single extracted blood sample. If biomarkers for each separate disorder were determined, calibration curves could be generated for each compound. From these curves, data could be taken by simply changing width and location of the isolation window and changing the frequency at which CID is performed. This would allow for a series of disorders to be screened for in succession without stopping to load a new sample or extracting and derivatizing multiple blood spots.

In addition to the analysis of low molecular weight drug molecules discussed in this dissertation, it is of interest to test the aerogel MALDI technique for the analysis of higher molecular weight compounds, such as peptides and

proteins For this the aerogel MALDI technique would have to be formatted onto an instrument capable of high-mass analysis like a time-of-flight mass spectrometer In addition different wavelength lasers could be tested and negative ion mass spectra could be investigated using aerogel MALDI

Furthermore the resorcinol-formaldehyde aerogels used in this study are only one type of aerogel produced Aerogels can be made with any monomers that can form a wet gel in the sol-gel process Due to the successful adaptation of RF aerogels to laser-based desorption-ionization mass spectrometry it would be of interest to study other aerogel system as well For example, an aerogel system could possibly be produced from monomers specifically designed to absorb the ultraviolet radiation from the nitrogen laser or other wavelengths more efficiently

Also it is possible to modify the surface of the pores by reaction after the original production of the aerogel This could be done by reactions similar to those described for porous silicon modification (Bunak & Allen 1998) However the application of solvent to the pore system for these reactions may have the negative effect of pore system collapse similar to that shown here If so other methods of surface modification could be examined

Finally the sensitivity of the aerogel MALDI technique is based on the amount of the analyte that the laser can desorb and ionize for each laser shot. In this case the analyte solution is deposited onto a surface that is nearly four millimeters wide If the sample surface was decreased in size and the laser spot size, the sample concentration and the amount of liquid sample deposited onto

the aerogel remained the same there would be a higher concentration of analyte on the aerogel surface That is there would be the same amount of analyte as before but it would be concentrated into a smaller space When the laser is then focused onto the aerogel surface it would be able to desorb and ionize more analyte for each laser shot This would allow for more dilute sample solutions to be detected due to the concentration of analyte within a more confined sample area and therefore increase the sensitivity of the aerogel MALDI technique

This could be done by use of a piezoelectric pipetter (Laurell *et al* 1999) Piezoelectric pipetters produce low-volume solvent droplets by the filling a reservoir with solvent and pumping it out a small nozzle by applying a controlled pressure on the side of the reservoir This is accomplished by placing a piezoceramic around the sample reservoir These ceramics contract when an electric potential is placed on it and small reproducible droplets are formed by applying a series of signals with a specific voltage, pulse width and frequency to the pipetter

If the aerogel system could handle the re-wetting of the pore system samples could be loaded into the piezopipetter and dropped on the aerogel surface in small spot sizes The sample could then be analyzed as described earlier However this would require visualization capabilities within the source of the mass spectrometer In order to insure that the laser is focused onto the spot where the sample was deposited The instrument used in this study did not have this capability and was therefore unable to perform studies of this nature

REFERENCES

Ahmed M S Attia Y A *J Non-Cryst Solids* **1995** *186* 402

Amato G Bullara V Brunetto N Boarino L *Thin Solid Films* **1996** *276* 204-207

Amato G Rosenbauer M *Optoelectronic Properties of Semiconductors and Superlattices* 3 52 Gordon and Breach Amsterdam 1997

Anderson D F Powell D H Smith, B W Winefordner J D *Proceedings of the 50th ASMS Conference on Mass Spectrometry and Allied Topics* Orlando FL **2002**

Barber M Bordoli R S Elliot G J Sedgwick R D Tyler A N *Anal Chem* **1982** *54* 645A

Beavis R C Chait B T *Proc Natl Acad Sci USA* **1990** 87 6973

Belford M W Yost R A *Proceedings of the 49th ASMS Conference on Mass Spectrometry and Allied Topics* Chicago IL **2001**

Bhattacharya S H Murray K K *Proceedings of the 50th ASMS Conference on Mass Spectrometry and Allied Topics* Orlando FL **2002**

Bier M E Schwartz J C *Electrospray Ionization Mass Spectrometry* R B

Bingham R A Salter P L *Anal Chem* **1975** *46* 1735-1739

Borum P R *Clinical Aspects of Human Carnitine Deficiency* 16-27 Pergamon Press New York 1986

Briand G Fontaine M Schubert, R Ricart G Degand P Varnecq, J J *Mass Spectrom.* **1995** *30* 1731-1741

Bunak J M Allen M J *J Am Chem Soc* **1998** *120*, 1339-1340

Canham L *Appl Phys Lett* **1990** *57* 1046-1048

Canham L T *Properties of Porous Silicon*, Institute of Electrical Engineers London 1997

Chace D Bennett M J Roe C R Save Babies Through Screening Webpage http //www savebabies org Last accessed November 15 2002

Chapman J R *Practical Organic Mass Spectrometry* 2nd Ed John Wiley & Sons New York **1994**

Chen Y T Millington D S Newborn Screening at Duke Webpage 2000

Cotter R J Doroshenko V M Cornish T J *Rapid Commun Mass Spectrom* **1992** *6* 753-757

Cotter R J Tabet J C *Amer Lab* **1984** *April* 86-98

Cotter R Heller D N Lys I Uy O M *Anal Chem* **1988** *61* 1083-1089

Cullis A G Canham L T Calcott P D J *J Appl Phys* **1997** 82 909-965

Dawson P H , Whetten N R "Three-Dimensional Mass Spectrometer and Gauge" *British Patent* 1 225 272, **1971**

Dawson P H Whetten N R *J Vac Sci Technol* **1968** *5* 11-18

Detter L D Hand O W Cooks R G , Walton R A *Mass Spectrom Rev* **1988** *7* 465

Elliman D A C Dezateux C Bedford H E *Arch Dis Child* **2002** 87 6-9

Engel A G Rebouche C J Wilson, D M Glasgow A M Romaine C A Cruse R P *Neurology* **1981** *31* 819-825

Fischer E *Z Phys* **1958** *156* 1-26

Fulford, J E Hoe D N Hughes R J March R E Bonner R F Wong, G J *J Vac Sci Technol* , **1980**, 17 829-835

Griffin, T Ph D Dissertation *GC/MS/MS on the Quadrupole Ion Trap Mass Spectrometer Software Development and the Examination of the Effects of Ion Population* University of Florida **1995**

Guthrie R Susi, A *Pediatric* **1963** 32 338

Henig K Henion J *J Chrom B* **1998** *735* 171-186

Henning, S *Springer Proceedings in Physics* **1986** *6* 38

Hercules D M Novak F P Viswanadham S K Wilk Z. A. *Anal Chem Acta* **1987** *193* 61-71

Herrmann G Iden R Mielke M Teich F Ziegler B *J Non-Cryst Solids* **1995** *186* 360

Honig R E Woolston J R *Appl Phys Lett* **1963** *2* 138-139

Hummel R E *Appl Phys Lett* **1992** *61* 1965 1967

Johnson J. V., Yost R A Kelley P E Bradford D C *Anal Chem* **1990** *62*, 2162

Johnson J Powell D Borum P *Proceedings of the 46th ASMS Conference on Mass Spectrometry and Allied Topics* Orlando FL **1998**

Jonscher K R Yates J R *Anal Biochem* **1997** *244* 1

Kagawa M Machida Y Nishi H *J Chrom A* **1999** *857* 127-135

Karas M Bahr U Giebmann U *Mass Spectrom Rev* **1991** *10* 335-357

Karas M Hillenkamp F *Anal Chem* **1988** *60* 2299-2301

Kalland D Wallach E. R. *Anal Chem Acta* **1987** *195* 89-96

Kistler S S *J Phys. Chem* **1932** *34* 52

Kistler S S *Nature* **1931** *127* 741

Kong F M *Low Density Carbonized Composite Foams* U S Patent 4 992 254 (Jan 12 1991)

Kruse R A., Li X Bohn P W Sweedler, J V *Anal Chem* **2001** *73*, 3639-3645

Kuhara T Shinka T Inuoe Y Ohse M Zhen-wei X Yoshida I Inokuchi T Yamaguchi S Takayanagi M Matsumoto I *J Chrom B* **1999**, *731* 141-147

Laurell T Wallman L Nilsson J *J Micromech Microeng* **1999** *9* 369-376
Lee M S Yost R *A Biomed Environ Mass Spectrom* **1988** *15*, 193-205

LeMay J D Hopper R W Hrubesh L W Pekala R W *MRS Bull* **19** *12* 30-36, December 1990

Li, G. M., Dillen, L., Laeys, M. *Biol. Mass Spectrom.* **1992**, *21*, 408.

Ligon, W. V., Dorn, S. B. *Int. J. Mass Spectrom. Ion Processes* **1984**, *57*, 75.

Louris, J. N., Amy, J. W., Ridley, T. Y., Cooks, R. G. *Int. J. Mass Sprectom. Ion Processes* **1989**, *89*, 97.

Louris, J. N., Cooks, R. G., Syka, J. E. P., Kelley, P. E., Stafford, G. C., Todd, J. F. J. *Anal. Chem.* **1987**, *59*, 1677.

Major, F. G., Dehmelt, H. G. *Phys. Rev.* **1968**, *170*, 91.

March, R. E., J. J. *Mass Spectrom.* **1997**, *32*, 350.

March, R. E., Todd, J. F. J. *Practical Aspects of Ion Trap Mass Spectrometry*, Vol. 1, CRC Press: New York, **1995**.

Mathieu, E. J. *J. Math. Pure Appl.* **1868**, *13*, 137.

McClellan, J. E., Quarmby, S. T., Yost, R. A., Borum, P. R. *Proceedings of the 45th ASMS Conference on Mass Spectrometry and Allied Topics*, Palm Springs, CA, **1997**.

McCrery, D. A., Gross, M. L. *Anal. Chem. Acta*, **1985**, *178*, 105-115.

Millington, D. S., Roe, C. R., Maltby, D. A. *Biomed. Mass Spec.* **1984**, *11*, 236-241.

Moon, D. C., Kelley, J. A. *Biomed. Environ. Mass Spectrom.* **1988**, *17*, 229.

Murphy, J. P., Ph.D. Dissertation, *Fundemental Studies of the Quadrupole Ion Trap Mass Spectrometer: Compound-Dependent Mass Shifts and Space Charge*, University of Florida, **2002**.

Murray, K. K., Bhattacharya, S. H., Little, M. W., Reiford, T. J. *Proceedings of the 50th ASMS Conference on Mass Spectrometry and Allied Topics*, Orlando, FL, **2002**.

O'Shea, D. C., Callen, W. R., Rhodes, W. T. *Introduction to Lasers and their Applications*, Addison-Wesley: Menlo Park, **1978**.

Paul, W., Steinwedel, H. "Apparatus for Separating Charged Particles of Different Specific Charges", *German Patent 944,900*, **1958**.

Pekala, R. W., Alviso, C. T., Kong, F. M., Hulsey, S. S. *J. Non-Cryst. Solids* **1992**, *145*, 90-98.

Pekala, R. W., Mayer, S. T., Kaschmitter, J. L., Kong, F. M. In *Sol-Gel Processing and Applications*; edited by Y. A. Attia; Plenum: New York, 1994; p 369.

Pekala, R. W., Stone, R. E. *Polymer Reprints* **1999**, *29*, 204.

Parchalski, R. J., Wilder, B. J., Yost, R. A. *Anal. Chem.* **1983**, *55*, 2002-2005.

Quarmby, S. T. Ph.D. Dissertation. *Fundamental Studies of Ion Injection and Trapping of Electrosprayed Ions on a Quadrupole Ion Trap Mass Spectrometer*. University of Florida: **1997**.

Quarmby, S. T., Yost, R. A. *Int. J. Mass Spectrom.* **1999**, *190/191*, 91.

Rebouche, C. J., Broquist, H. P. *J. Bacteriol.*, **1976**, *126*, 1207-1214.

Reddick, C. Ph.D. Dissertation. *The Detection of Pharmaceutical Drug Compounds from Intact Biological Tissue by Matrix assisted Laser Desorption Ionization (MALDI) Quadrupole Ion Trap Mass Spectrometry*. University of Florida: **1997**.

Sailor, M. J., Lee, E. J. *Adv. Mater.* **1997**, *9*, 783-793.

Schwartz, J. C., Bier, M. E. *Rapid Commun. Mass Spectrom.*, **1993**, *7*, 27-32.

Scott, C., Kosmidis, C., Jia, W., Ledingham, K., Singhal, R. *Rapid Commun. Mass Spectrom.* **1994**, *8*, 829-832.

Shen, Z., Thomas, J. J., Averbuj, C., Broo, K. M., Engelhard, M., Crowell, J. E., Finn, M. G., Siuzdak, G. *Anal. Chem.* **2001**, *73*, 612-619.

Shigematsu, Y., Hata, I., Kikawa, Y., Mayumi, M., Tenaka, Y., Sudo, M., Kado, N. *J. Chrom. B.* **1999**, *731*, 97-103.

Spengler, B., Cotter, R. J. *Anal. Chem.* **1990**, *62*, 793-799.

Spengler, B., Karas, M., Hillenkamp, F. *J. Phys. Chem.*, **1987**, *91*, 6502-6505.

Stafford, G. C., Kelley, P. E., Bradford, D. C. *Am. Lab.*, **1983**, 51-57.

Stafford, G. C., Kelley, P. E., Stephens, D. R. *U.S. Patent 4540884*, **1985**.

Stafford, G. C., Taylor, D. M., Bradshaw, S. C., Syka, J. E. P., Ulrich, M. *Proceedings of the 35th ASMS Conference on Mass Spectrometry and Allied Topics*. Denver, CO. **1997**. 775.

Stewart, M. P., Buriak, J. M. *Agnew. Chemie. Int. Ed.* **1999**, *37*, 3257.

Sun, C. C., Mark, J. E. *Polymer*. **1989**, *30*, 104.

Syka, J. E. P. *Practical Aspects of Ion Trap Mass Spectrometry*. March, R. E., Todd, J. F. J., Eds. CRC Press: Boca Raton, FL. 1995. Vol. 1, 185.

Tanaka, K., Waki, H., Ido, Y., Akita, S., Yoshida, Y., Yoshida, T. *Rapid Comm. MS*. **1988**, 151-153.

Troendle, F. J. Ph.D. Dissertation. *A Quadrupole Ion Trap Laser Microprobe for the Mapping of Pharmaceutical Compounds in Intact Tissue*. University of Florida. **2000**.

Tsou, P. *J. Non-Cryst. Solids*. **1995**, *186*, 415.

Tucker, D. B., Hasmeister, C. H., Bradshaw, S. C., Hoekman, D. J., Waber-Grabeu, M. *Proceedings of the 36th ASMS Conference on Mass Spectrometry and Allied Topics*. San Francisco, CA. **1999**. 828.

Uhlir, A. *Bell Syst. Tech. J.* **1959**, *35*, 333-347.

Varagnat, J. In "Encyclopedia of Chemical Technology" edited by H. F. Mark, D. F. Othmer, C. G. Overberger and G. T. Serborg. Wiley: New York. 1981. Vol. 13, p. 39.

Vargas, R. R. Ph.D. Dissertation. *Development of Laser Desorption Ionization on a Quadrupole Ion Trap Mass Spectrometer*. University of Florida. **1993**.

Vertes, A., Gijbels, R. Levine, R. *Rapid Commun. Mass Spectrom.* **1990**, *4*, 228-233.

Vertes, A., Irinyi, G., Gijbels, R. *Anal. Chem.* **1993**, *65*, 2389-2393.

Wang, S. S., Fernhoff, P. M., Hannon, W. H., Khoury, M. J. *Genetics in Medicine*. **1999**, *7*, 332-339.

Wei, J., Buriak, J. M., Siuzdak, G. *Nature*. **1999**, *399*, 243-246.

Werstler, D. D. *Polymer*. **1986**, *27*, 757.

Woffendin, G. *Thermo Finnigen Application Note 9119*. **1999**.

Wuerker, R. E., Shelton, H., Langmuir, R. V. *J. Appl. Phys.* **1959**, *30*, 342.

Yost, R. A., Boyd, R. K. *Methods in Enzymology* **1990**, *193*, 154.

Yost, R. A., Fetterolf, D. D. *Mass Spectrometry Reviews* **1983**, *2*, 1.

Zenobi, R., Knochenmuss, R. *Mass Spectrom. Rev.* **1998**, *17*, 337-366.

Zimmerman, A., Gross, J., Fricke, J. *J. Non-Cryst. Solids* **1995**, *186*, 238.

BIOGRAPHICAL SKETCH

Michael William Belford was born in Miami, Florida, on February 26, 1976. At age four, he and his family, now totaling five after the additions of his two younger brothers, Chris and Steven, moved to Altamonte Springs, Florida, where the family still resides. He met his future wife, Shana Wadsworth, while in high school there.

Michael left the state of Florida to attend Pfeiffer University in Misenheimer, North Carolina, after graduation from high school. At Pfeiffer, Michael played lacrosse, basketball and ran on the cross-country team while working on his degree in chemistry. In 1997, he discovered the joys of mass spectrometry while attending a summer undergraduate research program under the supervision of Dr. Ken Marcus at Clemson University, where he built a time-of-flight instrument.

After graduation from Pfeiffer in 1998, Michael and Shana were married and moved to Gainesville to start graduate school at the University of Florida. While in Gainesville, Michael worked under the supervision of Dr. Richard Yost and focused on the workings of the quadrupole ion trap mass spectrometer and the development of porous polymeric surfaces for laser desorption.

In December of 2001, Shana and Michael welcomed William Jacob into the world and have been trying to catch up with him ever since.

I certify that I have read this study and that in my opinion it conforms to acceptable standards of scholarly presentation and is fully adequate in scope and quality as a dissertation for the degree of Doctor of Philosophy

Richard A Yost Chair
Professor of Chemistry

I certify that I have read this study and that in my opinion it conforms to acceptable standards of scholarly presentation and is fully adequate in scope and quality as a dissertation for the degree of Doctor of Philosophy

John R Eyler
Professor of Chemistry

I certify that I have read this study and that in my opinion it conforms to acceptable standards of scholarly presentation and is fully adequate in scope and quality as a dissertation for the degree of Doctor of Philosophy

David H Powell
Scientist of Chemistry

I certify that I have read this study and that in my opinion it conforms to acceptable standards of scholarly presentation and is fully adequate in scope and quality as a dissertation for the degree of Doctor of Philosophy

James D Winefordner
Graduate Research Professor of
Chemistry

I certify that I have read this study and that in my opinion it conforms to acceptable standards of scholarly presentation and is fully adequate in scope and quality as a dissertation for the degree of Doctor of Philosophy

Bruce A Goldberger
Clinical Assistant Professor of
Pathology Immunology and Laboratory
Medicine

This dissertation was submitted to the Graduate Faculty of the Department of Chemistry in the College of Liberal Arts and Sciences and to the Graduate School and was accepted as partial fulfillment of the requirements for the degree of Doctor of Philosophy

May 2003

_____

Dean Graduate School